1-1-2016

AKAP150 Dynamics in Anterior Pituitary Cells

Kristen E. Dew
University of Denver

AKAP150 Dynamics in Anterior Pituitary Cells

Abstract

Cellular communication occurs as a result of changes in signaling pathways. A well-studied signaling pathway is through G protein coupled receptors (GPCRs). In gonadotropes, GPCR stimulation by GnRH leads to the activation of protein kinase A (PKA). Activated PKA can phosphorylate ion channels, potentially causing an influx of calcium, depolarization and secretion of hormones. A scaffolding protein known as AKAP150 anchors PKA near L-type calcium channels. In addition, AKAP150 anchors phosphatases, which provides temporal control during signaling events. It was recently shown that AKAP150 is mobile in neuronal dendrites, providing regulation to where the signaling cascade occurs in the cell. It is not yet known what AKAP150 binds to in gonadotropes or how it translocates. In order to investigate the mobility of this protein in pituitary cells, a variety of methods were used in this study. Time-lapse imaging and permeabilization assays suggested that AKAP150-GFP was mobile in LbetaT2 cells, but more sensitive methods were needed to study temporal and spatial resolution. Quantitative FRAP and FLIP analysis provided strong qualitative evidence that AKAP150-GFP was mobile in LbetaT2 cells and the protein moved laterally along the cell rim. Lastly, comparing rim intensity in LbetaT2 cells immunostained for endogenous AKAP150 and actin indicated the scaffolding protein could cluster with to actin.

Document Type

Thesis

Degree Name

M.S.

Department

Biological Sciences

First Advisor

Joseph K. Angleson, Ph.D.

Second Advisor

Scott Barbee

Third Advisor

Nancy Lorenzon

Keywords

AKAP150, Anterior pituitary cells, Fluorescence recovery after photobleaching, FRAP, Gonadotropes, LβT2 cells

Subject Categories

Biology | Cell Biology | Molecular Biology

AKAP150 Dynamics in Anterior Pituitary Cells

A Thesis

Presented to

the Faculty of Natural Sciences and Mathematics

University of Denver

In Partial Fulfillment

of the Requirements for the Degree

Master of Science

by

Kristen E. Dew

June 2016

Advisor: Dr. Joseph K. Angleson, Ph.D.

Author: Kristen E. Dew
Title: AKAP150 Dynamics in Anterior Pituitary Cells
Advisor: Dr. Joseph K. Angleson, Ph.D.
Degree Date: June 2016

ABSTRACT

Cellular communication occurs as a result of changes in signaling pathways. A well-studied signaling pathway is through G protein coupled receptors (GPCRs). In gonadotropes, GPCR stimulation by GnRH leads to the activation of protein kinase A (PKA). Activated PKA can phosphorylate ion channels, potentially causing an influx of calcium, depolarization and secretion of hormones. A scaffolding protein known as AKAP150 anchors PKA near L-type calcium channels. In addition, AKAP150 anchors phosphatases, which provides temporal control during signaling events. It was recently shown that AKAP150 is mobile in neuronal dendrites, providing regulation to where the signaling cascade occurs in the cell. It is not yet known what AKAP150 binds to in gonadotropes or how it translocates. In order to investigate the mobility of this protein in pituitary cells, a variety of methods were used in this study. Time-lapse imaging and permeabilization assays suggested that AKAP150-GFP was mobile in LβT2 cells, but more sensitive methods were needed to study temporal and spatial resolution. Quantitative FRAP and FLIP analysis provided strong qualitative evidence that AKAP150-GFP was mobile in LβT2 cells and the protein moved laterally along the cell rim. Lastly, comparing rim intensity in LβT2 cells immunostained for endogenous AKAP150 and actin indicated the scaffolding protein could cluster with to actin.

ACKNOWLEDGMENTS

Foremost, I would like to thank my advisor, Dr. Joseph K. Angleson, for this research opportunity. I have appreciated your guidance, support and advice. Your enthusiasm when interpreting results helped me to realize the excitement found in research. I would like to thanks the members of my committee: Dr. Scott A. Barbee and Dr. Nancy M. Lorenzon for supporting me through this process and providing helpful advice in order to graduate. I would like to thank my collaborators: Dr. Dinah Loerke and Roopa Madhu for your insight and patience when analyzing FRAP data. My lab mates, Larissa Ikenouye and Emily Wilkinson, thank you for your support and providing an enjoyable place to work. To Larissa, thank you for always being willing to teach me lab techniques. I have learned a lot from you and strive to replicate your willingness to help others. I am appreciative of my fellow graduate students for helping me through classes and providing fun memories from T.A. meetings. Furthermore, to my family and friends, thank you for your encouragement and support. To Alexi and Grace Tombaugh, thank you for taking great care of Graham so I could finish this program. Special thanks to my husband, Steve Dew, for being my rock through this journey. Your love and encouragement kept me going each day. Lastly, special thanks to my son, Graham Dew, for providing me with the joy of becoming your mom.

TABLE OF CONTENTS

LIST OF FIGURES

INTRODUCTION

Basic Hormone Function

One role of the endocrine system in the human body is to maintain body homeostasis by signaling through hormones. Hormones are chemical signals that help to coordinate the body's functions. When released from a cell, peptide hormones are secreted into the blood stream and control long lasting responses to stimuli in the body. Examples of stimuli affecting the endocrine system include dehydration, low blood glucose levels and an increase in heart rate and stress when feeling threatened (Yeung et al. 2006). In addition to regulating the response to specific stimuli, hormones control developmental processes such as distinct sex-driven appearances between adult males and females. Several disease states exist due to an imbalance of hormones. A few of these diseases include diabetes mellitus, hypopituitarism, Cushing syndrome and Graves' disease. Peptide hormones are composed of protein, peptides, or amines and are compacted in dense core vesicles before being released into the blood stream. Such hormones are soluble in water and are unable to pass through the cell membrane, thus requiring binding to a receptor on the outside of the cell to relay the signal to inside of the cell (Yeung et al. 2006).

A structure in the brain that controls the pituitary endocrine system is the hypothalamus. The hypothalamus receives signals from external and internal stimuli before sending out neuronal or hormonal responses. The hypothalamus affects the

endocrine system by directly stimulating or inhibiting the pituitary gland. The pituitary gland is composed of an anterior and posterior lobe. The anterior lobe contains endocrine cells and the posterior lobe is composed of nervous tissue and is considered an extension of the hypothalamus (Davis et al. 2013). The hypothalamus controls the anterior pituitary by using releasing and inhibiting hormones. The releasing hormones stimulate the anterior pituitary to secrete one or more specific hormones. The inhibiting hormones induce the anterior pituitary to stop secreting one or more specific hormones (Yeung et al. 2006).

The anterior lobe of the pituitary is composed of five different endocrine cell types that secrete hormones necessary for growth, development, metabolism and sexual function. These cell types include thyrotropes, lactotropes, corticotropes, somatotropes and gonadotropes (Ooi, Tawadros, and Escalona 2004). These cells secrete hormones directly into the blood, which control the activity of other endocrine glands and tissues.

Gonadotropes make up approximately 10-15% of the cell population in the anterior pituitary and secrete the gonadotropin hormones, leutinizing hormone (LH) and follicle-stimulating hormone (FSH). Gonadotropin secretion occurs when gonadotropin-releasing hormone (GnRH), binds to a GnRH- receptor, causing an increase in cytosolic calcium and secretion of LH and FSH (Ooi, Tawadros, and Escalona 2004). LH and FSH affect reproduction function by acting on the gonads. Once stimulated by LH or FSH, the ovaries and testes can then synthesize and secrete estrogens, progestins and androgens (Yeung et al. 2006).

LβT2 Gonadotrope cell line

In order to study gonadotropes as an isolated cell, several gonadotroph cell lines have been created. The present research study utilized the LβT2 immortalized cell line. The LβT2 cell line was created from pituitary tumors that developed in a transgenic mouse using the SV 40 T-antigen driven by the rat LHβ gene promoter. This cell line is considered an acceptable gonadotroph model because it expresses mRNA for both LHα and LHβ subunits, which are markers of gonadotrope differentiation (Ooi, Tawadros, and Escalona 2004). In addition, LβT2 cells express mRNA for the GnRH receptor and secrete LH when GnRH is bound to the GnRH receptor (Thomas et al. 1996). In addition, LH secretion is stimulated by depolarization of these cells, which is another indicator of the cell responding in a normal physiological manner.

In LβT2 cells, the GnRH receptor is a plasma membrane G protein coupled receptor (GPCR) that interacts with heterotrimeric G proteins to initiate downstream signaling (Liu et al. 2002). After the GTP-bound α subunit is released from the βδ subunits of the heterotrimeric G protein, several second messenger signaling molecules are activated. These molecules create an increase in intracellular diacylglycerol (DAG) and calcium from phosphoinositide turnover as well as an increase in intracellular cyclic adenosine monophosphate (cAMP) levels. The second messenger molecules then activate down-stream kinases, such as protein kinase C (PKC), protein kinase A (PKA), and calcium-dependent kinases (Liu et al. 2002). Specifically, GnRH activates the ERK, c-Jun N-terminal and p38 MAPK families in

LBetaT2 cells. GnRH also induces c-fos and LHβ protein expression in this cell line (Liu et al. 2002). The stimulatory G proteins coupled to the GPCR when activated by GnRH in LBetaT2 cells are $G\alpha_{q/11}$ and $G\alpha_{s.}$ To verify that these proteins were activated in LBetaT2 cells, recombinant adenovirus vectors expressing $G\alpha_q$ wildtype or a constitutively active mutant (Q209L) $G\alpha_q$ were used to analyze for increased ERK, c-Fos and LHβ protein expression. In the cells containing the constitutively active mutant, c-Fos and LHβ protein expression was induced, but ERK was not. The lack of ERK can be attributed to the protein becoming inactivated before expression could be detected. In addition, several peptides were created to specifically block $G\alpha_{q,}$ $G\alpha_s$ and Gβδ when measuring phospho-ERK expression in LβT2 cells after treatment with GnRH. The peptides successfully inhibited phospho-ERK expression by blocking $G\alpha_q$ and $G\alpha_{s,}$ but not Gβδ, indicating that signaling is occurring through $G\alpha_q$ and $G\alpha_{s.}$ (Liu et al.). The G protein coupled receptor does not activate $G\alpha_{i/o.}$ This was examined by blotting for phosphorylated ERK after treating the cells with pertussis toxin, a chemical known to stimulate $G\alpha_i$. After treatment with pertussis toxin, LBetaT2 cells did not show increased levels of phosphorylated ERK compared to control cells (Liu et al. 2002).

Basic Cellular Communication

Cellular communication is essential in multicellular organisms to coordinate activities for survival and growth. In order to communicate, cells must interpret extracellular ligands using receptors that form an intracellular protein cascade, which

creates the necessary cellular response. Examples of effector protein targets include gene regulatory proteins, ion channels, components of a metabolic pathway and cytoskeletal components (Hall and Lefkowitz 2002). By using extracellular signals for communication, this allows the cell to interact with other cells either nearby or far away in the organism. Endocrine cells secrete hormones into the blood stream to signal to other cells. Secreting hormones into the blood stream allows the endocrine cell to communicate with cells either nearby or very far away in the body.

In order for a cell to receive a signal, it must contain a receptor that recognizes the signal. Signaling ligands include proteins, small peptides, amino acids, and nucleotides (Kobilka 2007). Once an extracellular receptor has been activated, the signal is relayed through the cell by using small molecules and intracellular signaling proteins. Three of the most common small molecules include cyclic AMP (cAMP), calcium (Ca^{+2}) and diacylglycerol (DAG). These small signaling molecules help to relay the signal by binding to and altering the conformation or behavior of proteins involved in the signaling cascade. The proteins involved in the signaling cascade are usually intracellular proteins and help to progress or stop the signal by creating intermediate signaling molecules or changing the conformation of proteins in the signaling cascade (Brogi et al. 2014). The rate at which the changes are made in the cell receiving the signal vary depending on the desired outcome of the message received. Phosphorylation of a protein that is already in the cell occurs quickly while creation of a new protein or molecule through transcription and translation can take longer (Alberts, B. Johnson, A. Lewis, J. Raff, M. Roberts, K. Walter 2008).

G Protein Coupled Receptors

In many cells, messages are relayed from the extracellular space to the cytoplasm through G-protein coupled receptors (GPCRs). The function of activated GPCRs is to stimulate or inhibit other proteins in a signal transduction cascade or regulate an ion channel. The signals that the receptor receives include hormones, neurotransmitters, and local mediators. G protein coupled receptors are important to understand in the context of cell signaling because half of all known drugs work through these receptors (Alberts, B. Johnson, A. Lewis, J. Raff, M. Roberts, K. Walter 2008). GPCRs are a transmembrane protein that spans through the membrane seven times and is coupled with a trimeric GTP-binding protein. The GTP-binding protein is composed of alpha, beta and gamma subunits. In an inactive state, the alpha subunit has GDP bound to it and the subunits are congregated together. In an activated state, the alpha subunit dissociates from the trimeric protein and has GTP bound to it. There are several different isoforms of the alpha subunit, some of which are stimulatory and some of which are inhibitory (Alberts, B. Johnson, A. Lewis, J. Raff, M. Roberts, K. Walter 2008).

In LBetaT2 cells, the purpose of signaling through a GPCR is to increase the amount of cyclic AMP (cAMP) in order to activate protein kinase A (PKA). When the extracellular portion of the receptor binds a ligand, the receptor undergoes a conformational change, which allows it to activate the G protein, releasing the alpha subunit bound to GTP. The stimulated G alpha subunit then activates adenylyl cyclase (AC), another transmembrane protein. Adenylyl cyclase synthesizes cAMP

from ATP. The cAMP then binds to PKA in order to activate serine/threonine kinases (Alberts, B. Johnson, A. Lewis, J. Raff, M. Roberts, K. Walter 2008).

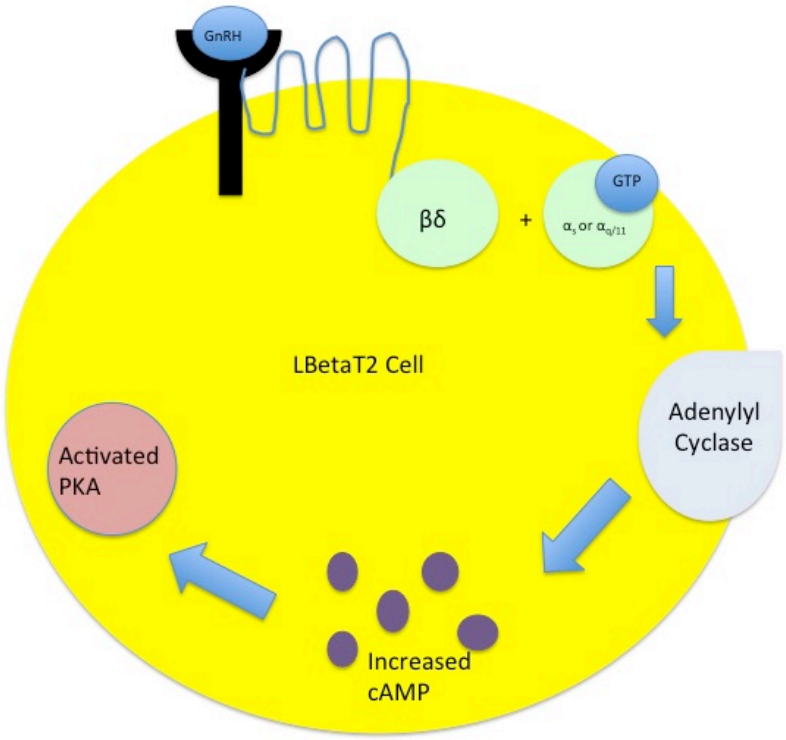

Figure 1: Signaling cascade leading to the activation of protein kinase A. When the hormone GnRH, binds to the GnRH receptor, the α subunit of the trimeric GTP binding protein, becomes activated and dissociates from the βδ subunits. The GTP-bound α subunit activates adenylyl cyclase, leading to an increased concentration of intracellular cAMP. The increased concentration of cAMP activates PKA, which can then phosphorylate serine and threonine residues on proteins.

Protein Kinase A

Protein Kinase A, or PKA, is an enzyme that regulates many biological processes and is associated with disease due to insufficient or inappropriate phosphorylation (Taylor et al. 2012). Protein Kinase A is a holoenzyme consisting of two regulatory subunits and two catalytic subunits. The regulatory subunits include RIα, RIβ, RIIα and RIIβ. The different catalytic subunits include Cα, β, and δ (Dell'Acqua and Scott 1997). The regulatory and catalytic subunit isoforms allow for the formation of different isoforms of the holoenzyme, which bind to specific subcellular locations in the cell. PKA I is primarily found in the cytoplasm where as PKA II is targeted mainly to subcellular structures (Taskén and Aandahl 2004). The regulatory subunits each contain two binding sites for cAMP. The two sites on the regulatory subunit where cAMP can bind are the A site and B site. cAMP binds to the B site first and then the A site (Taskén and Aandahl 2004). When cAMP is not bound to the regulatory subunits the enzyme is inactive. Once the cAMP has bound to the regulatory subunits, then the catalytic subunits are released from the holoenzyme and are free to phosphorylate on serine or threonine residues on several different protein substrates (Taskén and Aandahl 2004). Phosphorylation of serine or threonine residues on specific proteins induce conformational changes that activate or inhibit cellular processes. In cardiac cells, phosphorylation of L-type calcium channels by PKA enhances the influx of calcium and depolarization of the cell (Gao et al. 1997). In gonadotrophs, phosphorylation and enhanced opening of ion channels could lead to increased calcium influx, depolarization and secretion of hormones (Dell'Acqua and Scott 1997).

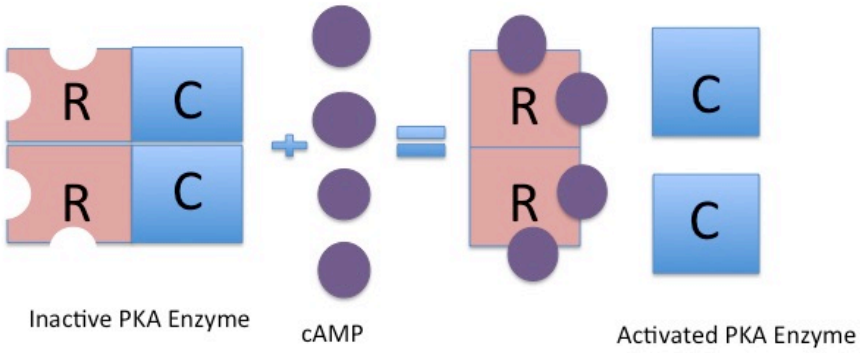

Figure 2: A model demonstrating the activation of protein kinase A. Protein kinase A is a holoenzyme consisting of two regulatory (R) subunits and two catalytic (C) subunits. In an inactive state, cAMP is not bound to the holoenzyme. In an activated state, the regulatory subunits bind cAMP and the catalytic subunits dissociate from the regulatory subunits. The catalytic subunits can then phosphorylate threonine and serine residues on proteins.

AKAP150

A Kinase Anchoring Proteins (AKAPs) are scaffolding proteins that can bind both kinases and phosphatases. By localizing kinases and phosphatases in close proximity to each other allows for greater temporal control in signaling cascades (Dai, Hall, and Hell 2009). AKAP150 is one of the most studied anchoring proteins in neuronal and cardiac cells. AKAP150 is expressed in mice and has two orthologs: AKAP75 in bovine and AKAP79 in humans (Tunquist et al. 2008). The enzymes most commonly bound to AKAP150 are PKA, calcium/phospholipid-dependent protein kinase C (PKC) and calcium/calmodulin-dependent protein phosphatase 2B (PP2B). Each of the enzymes is inhibited when bound to the AKAP and requires specific second messenger signals to activate the enzymes. The scaffolding complex is tethered to the interior of the plasma membrane where its binding partner can respond to second messengers, such as cAMP, calcium, and phospholipids. When bound to the interior of the plasma membrane, the AKAP 150 family of proteins controls phosphorylation of ion channels such as AMPA-type glutamate receptors, L-type calcium channels, aquaporin water channels and M-type potassium channels (Hoshi, Langeberg, and Scott 2005). By anchoring signaling enzymes in such close proximity, enzyme regulation can be partially controlled by negative feedback loops. For example, in addition to phosphorylating substrates, increased PKA activity activates PP2B, which dephosphorylates the substrate targeted by PKA. In neurons, AKAP 150 is targeted to post-synaptic densities (Hoshi, Langeberg, and Scott 2005). The post-synaptic substrates include α-amino-3-hydroxy-5-methyl-4-isoxazolepropionic acid (AMPA) receptors, calcium channels and N-Methyl-D-

aspartic acid (NMDA) receptors in hippocampal synapses (Taskén and Aandahl 2004). In studies involving Human Embryonic Kidney (HEK) cells and native cardiac myoctes, it was shown that PKA anchored to AKAP150 is necessary for the phosphorylation of α_{1C} subunits in maintaining an open state of L-type calcium channels (Gao et al. 1997). In cardiac myocytes, stimulation of L-type calcium channels by β-adrenergic agonists occurs through a cAMP and PKA-dependent pathway. Disruption of this pathway by blocking the ability of PKA to bind to AKAP150 results in reduced calcium channel currents (Gao et al. 1997). In addition to anchoring PKA, PKC and PP2B, it has been proposed that AKAP150 interacts with F-actin, phosphatidylinositol-4,5-bisphosphate (PIP_2) and cadherin complexes to anchor the protein in post synaptic densities in neurons. This has been proposed because the scaffold has been shown to be disrupted by actin polymerization inhibitors (Dell'Acqua et al. 2006). Due to the unknown nature of what AKAP150 is binding to, there is not much information about how the protein translocates. The aim of my thesis is to generate more knowledge about the binding and translocation of AKAP150 in anterior pituitary cells.

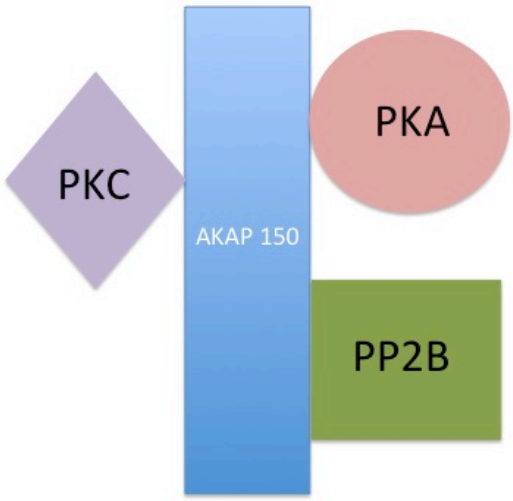

Figure 3: AKAP150 scaffolding protein model. The three most common enzymes attached to the AKAP150 scaffolding protein are protein kinase A (PKA), protein kinase C (PKC) and the calcium/calmodulin-dependent protein phosphatase 2B (PP2B).

Intent of Thesis

The goal of this thesis is to study the dynamics of AKAP150 in anterior pituitary cells. AKAP150 is dynamic protein in the dendritic spines of neuronal cells: AKAP150 can bind lipids in the cell membrane and actin in the cytoskeleton (Dell'Acqua et al. 2006). However how the protein translocates and what causes it to translocate is currently not known. Previous preliminary experiments conducted in the Angleson lab suggest cortical localization of AKAP150 in endocrine cells changes with treatment of pharmacological agents. We investigated these changes using time-lapse imaging, FRAP, FLIP, and immunostaining assays. During this process, we also demonstrated method development for analyzing quantitative FRAP data. Using these methods allowed us to learn more about the dynamics of AKAP150 in anterior pituitary cells.

MATERIALS AND METHODS

Cell Culture

LBetaT2 cells from Pamela Mellon (University of California, San Diego) were cultured in DMEM media containing 25mM glucose (Cellgro), 1% sodium pyruvate (Cellgro), 10% fetal bovine serum (Valley Biomedical), 1% of a penicillin/streptomyocin solution (10,000 IU/mL Penicillin, 10,000 ug/mL Streptomyocin, Cellgro) and 1.85g sodium bicarbonate (Fisher Scientific). All ingredients were mixed together and brought up to 500mL with nanopure water. The media was sterilize filtered with a 0.45μm filter (Cell treat). The cells were maintained in a humidified incubator with 95% air, 5% CO_2 at 37°C. The cells were split approximately once every seven to ten days.

The 5mM K^+ standard external resting solution used during experiments contained 1mM $MgCl_2$, 10mM HEPES, 5mM $CaCl_2$, 137mM NaCl, 5mM KCl and 10mM D-glucose (pH 7.2). The high potassium solution contained 1mM $MgCl_2$, 10mM HEPES, 5mM $CaCl_2$, 42mM NaCl, 100mM KCl and 10mM D-glucose (pH 7.2).

Plating Cells

Chamber slides were coated with 250μL ECL (EMD Millipore), a cell adhesion matrix, and incubated at 37°C for 90 minutes. Media was removed from a

flask containing LβT2 cells and pipetted into a 50mL conical tube. 5ml trypsin (Corning) was added to flask for three minutes. Each side of the flask was washed with trypsin and then trypsin was pipetted into the bottom several times to break up clumps of cells. The cells (and trypsin) were added to the 50mL conical and centrifuged at 5000rpm for 10 minutes. The supernatant was removed from the cell pellet and LβT2 media was used to re-suspend the cells. ECL was removed from the chamber slides and 500μL of cells were added to each chamber. Cells were incubated at 37°C for 45 minutes.

Plasmid Preps

The AKAP150-GFP plasmid (gift from Mark Dell'Acqua) was isolated using competent DH5α *E. coli* cells (Invitrogen). AKAP150-GFP (1μL) plasmid was added to chilled DH5α cells (100μL) and incubated on ice for 30 minutes. The cells were heat shocked at 42°C for 50 seconds and then incubated on ice for two minutes. S.O.C. media (900μL) (Invitrogen) was added to the cells and shaken at 225rpm for 1 hour at 37°C. Transformed cells (10μL) were added to 990μL S.O.C. media (Invitrogen) and 100μL of that solution was spread on a LB plate containing kanamycin. The plate was incubated overnight at 37°C. One colony was removed on a plate with a 200mL pipette tip and added to LB broth (110mL) containing 110μL kanamycin (50mg/mL). The flask was shaken overnight at 37°C at 300rpm. A Qiagen maxi plasmid prep kit was used for eluting plasmid from *E. coli*. The plasmid (1μg/μL) was diluted with endotoxin-free TE Buffer.

Transfection of LβT2 Cells

Glass bottom dishes (17mm thick, Wellco) were coated with ECL (300μL) and put in incubator at 37°C for 1 hour. Opti-Mem or TransfectaGro (1mL) was warmed to room temperature in a 37°C water bath. Opti-MEM (200μL) was pipetted into a 1.5mL tube labeled A and into a 1.5mL tube label B. Lipofectamine Reagent 2000 (2μL) was added to tube A. 2μL endotoxin-free AKAP150-GFP plasmid (1405.2ng/μL) was added to tube B. The reactions incubated at room temperature for 5 minutes. Tube A was added to tube B and the reaction was incubated at room temperature for 20 minutes. Media was pipetted from the flask and placed in a 50mL centrifuge tube. Cells were treated with trypsin for three minutes. Each side of the flask was washed with trypsin and then trypsin was pipetted into the bottom several times to break up clumps of cells. Cells (and trypsin) were centrifuged at 5000rpm for 10 minutes and supernatant was removed from the cell pellet. Cells were re-suspended in Opti-Mem (100μL). ECL was removed from the glass bottom dishes and re-suspended cells (25μL) were added to each dish. 100μL from the tube containing lipofectamine, Opti-MEM and plasmid was added to the cells on the glass bottom dish. The glass bottom dishes were incubated for three hours in an incubator at 37°C and containing 95% air and 5% CO_2. LβT2 media (2mL) was added to each dish and then the incubation at 37°C continued for either 24 or 48 hours.

Time-lapse Imaging Assay

Perfusion assays were performed using a gravity flow system. One image was taken every 30 seconds for approximately 10 minutes (20 time points). Perfusion solutions contained either a standard external solution or the standard resting solution with a pharmacological agent, added as indicated. The standard resting solution was 5mM K^+/10mM glucose. The starting solution for LβT2 cells transfected with AKAP150-GFP plasmid was the standard external solution. LβT2 cells transfected with AKAP150-GFP were perfused with the standard resting solution for the first two minutes of data collection. Immediately after two minutes, the solution was switched from resting solution to the solution containing a pharmacological agent for 30-60 seconds. After 30-60 seconds, the drug solution was turned off, and the cells were bathed in the solution containing a pharmacological agent for the remainder of the imaging. The intensities of the cell surface ('rim') were determined by subtracting a mask created by background signal from a mask created around the rim of a cell.

Permeabilization Assay

Chamber slides (Nalge Nunc International) were coated with ECL (250μL) and incubated at 37°C for 90 minutes. ECL was removed from slides and 500μL of LβT2 cells transfected with AKAP150-GFP were added to each chamber. Cells on chamber slides were incubated at 37°C for 45 minutes. The media was removed, and the cells were washed three times with phosphate buffered saline solution (PBS). A 4% paraformaldehyde (PFA) solution (Electron Microscopy Solutions) was added to

the cells for 15 minutes. The PFA solution was removed, and the cells were washed three times with PBS. To permeabilize cell membranes, a 0.4% Triton X-100 (Fisher Scientific) solution was added to the cells for 15 minutes. The Triton X-100 solution was removed, and the cells were washed three times with PBS. The chambers were removed from the slides and one drop of Vectashield with DAPI (Vector Laboratories, Inc.) was added to each space containing cells. Glass coverslips (Fisher Scientific, 18x18-3) were placed on top of the Vectashield and secured in place using clear nail polish. The intensities of the cell surface ('rim') were determined by subtracting a mask created by background signal from a mask created around the rim of a cell. For 'intact cell' preparation, permeabilization with Triton X-100 was omitted.

Immunostaining

LβT2 cells were plated on chamber slides. The media was removed and the cells were washed three times with PBS. A 4% paraformaldehyde (PFA) solution (Electron Microscopy Solutions) was added to the cells for 15 minutes. The PFA solution was removed, and the cells were washed three times with PBS. A 0.4% Triton X-100 solution was added to the cells for 15 minutes. The cells were washed three times with PBS. A 1:100 primary antibody solution was made with AKAP150 primary antibody (Goat anti-AKAP150, Santa Cruz Biotechnology, Catalog #: SC-6445) and blocking solution, normal donkey serum. The cells were incubated with the primary antibody solution at 37°C for 90 minutes in a humidifying chamber. The antibody was removed, and the cells were washed three times with PBS. A 1:800

secondary antibody solution (Alexa 488 anti-goat, Invitrogen) was made by pipetting secondary antibody into blocking solution with normal donkey serum. The cells were incubated with the secondary antibody solution at 37°C for 45 minutes in a humidifying chamber. The cells were washed three times with PBS. The chambers were removed from the slides, and one drop of Vectashield with DAPI was added to each space containing cells. Glass coverslips were secured in place using clear nail polish. In the cell containing drug treatment, the pharmacological agents were added for five minutes. The pharmacological agents were added after the media was removed, but before fixing the cells. In order to analyze endogenous AKAP150 and actin together, Alexa 568 phalloidin was added to the cells after the secondary antibody, and then the cells were incubated for 20 minutes in a humidifying chamber.

Fluorescence Microscopy

Fluorescence microscopy was performed using an inverted Zeiss Axiovert S100 TV microscope and recorded with Slidebook version 6.0 digital microscopy software. Images were acquired with 40x objective (N.A. 1.30). In the Slidebook software, images were viewed in the focus window with 40x oil objective, exposure of 1000ms, filter set to Live and the green Live filter was used. Images were acquired in the capture window with bin factor 1x1 and time lapse.

Confocal Microscopy

Confocal microscopy was performed using a laser scanning Olympus FluoView FV1000. Fluorescence Recovery After Photobleaching (FRAP) was done

on single LβT2 cells transfected with AKAP150-GFP using the Fluoview SIM scanner with Olympus Fluoview Ver 4.1 software. 550 images were acquired for each video using the 60x objective (N.A. 1.42) and Main Scanner Sync in Fluoview. The images of the cells were acquired using 5% laser transmission at wavelength 488 and the EGFP filter. The cells were photo bleached using 100% laser transmission at wavelength 488 and the EGFP filter. The tornado or rectangle tool was used to draw the region of interest (ROI) on the cell. Brightfield images were taken using 5% laser transmission at wavelength 488 and TD1 filter. Before imaging either cell type, media was removed and replaced with 5mM K^+ standard external resting solution.

Translocation of AKAP150-GFP was measured by creating recovery curves at the right, middle and left edges of the ROIs on the rim during photobleaching. When photobleaching using the baseline parameters, 0.5 microns were measured outside of the left and right edges of the ROI. 0.25 microns were measured on either side of the median in the middle of the ROI. When photobleaching using the fast rectangular and tornado parameters, 0.5 microns were measured outside of the left and right edges of the ROIs on the rim during photobleaching. 0.25 microns were measured on either side of the median in the middle of the ROI.

Confocal microscopy was performed on LβT2 single cells immunostained with anti-AKAP150 and phalloidin. AKAP150 was imaged with the Alexa 488 laser with 5% transmission. Actin was imaged with the Alexa 568 laser set to 5% transmission.

FRAP Analysis

Baseline parameters: A total of 300 frames were acquired at a frame rate of 1.11 seconds per frame for a total time of approximately 5.5 minutes. The rectangular ROI was bleached for 5 seconds at a speed of 100μs per pixel using 100% transmission of the 488 laser. The image was acquired using an aspect ratio of 512x512 at a speed of 12.5μs per pixel. The main scanner sync was used to collect images. 10 frames were taken before photobleaching. Images were acquired for 11 seconds, photobleached for 5 seconds and captured the recovery for 5.2 minutes.

Fast Rectangle parameters: A total of 550 images were acquired at a frame rate of 0.3 seconds per frame for a total time of approximately 2.75 minutes. The ROI was photobleached for either one second or 2.5 seconds at a speed of 100μs per pixel using 100% transmission of the 488 laser. Images were acquired using an aspect ratio of 128x128 at a speed of 2μs per pixel. The main scanner sync was used to collect images. 30 frames were taken before photobleaching. A rectangle ROI (13x49) was used in each experiment and positioned vertically around the cell rim. Images were acquired for 9 seconds, photobleached for either 0.3 seconds or 0.75 seconds and captured the recovery for approximately 2.5 minutes.

Fast tornado parameters: A total of 550 images were acquired at a frame rate of 0.3 seconds per frame for a total time of approximately 2.75 seconds. The ROI was photobleached for either one second or 2.5 seconds at a speed of 100μs per pixel using 100% transmission of the 488 laser. Images were acquired using an aspect ratio of 128x128 at a speed of 2μs per pixel. The main scanner sync was used to collect

images. 30 frames were acquired before photobleaching. A tornado ROI (22x22) was used in each experiment. Images were acquired for 9 seconds, photobleached for either 0.3 seconds or 0.75 seconds and captured the recovery for approximately 2.5 minutes.

Quantitative FRAP analysis was provided by Dr. Dinah Loerke and Roopa Madhu. Watershed analysis was used to define the rim of the cell and MATLAB was used to generate rim intensity. Rim intensity in the heat maps was calculated by dividing intensity at a point in time by the pre-bleach intensity. A red color indicates a value of 1, or maximum intensity. A blue color indicates a value of 0, or zero intensity.

Statistical Analysis

Slidebook Version 6.0 was used to create masks to analyze rim brightness in the time-lapse imaging, permeabilization, and immunostaining assays. Kaleidograph was used to create dot plots and run statistical analyses. Wilcoxon-Rank-Sum tests were used on non-normal distributions. Student's t-tests were run on normal distributions. Statistical significance was considered at $p<0.05$. Where indicated, data have been normalized to the third control time point and shown as mean and standard deviation.

Drug	Function	Working Concentration	Stock Concentration	Stock Solvent
Rp-8-CPT-cAMPs	Selective inhibitor of Protein Kinase A type I and II. Competitive inhibitor of PKA.	50μM	25mM	DMSO
6-benzoyl-cAMP	Activates Protein Kinase A type I and type II.	20μM	10mM	Water
Pimaric Acid (PiMA)	Activates Protein Kinase C	300nm	3.24mM	DMSO
Forskolin	Activates adenylyl cyclase	50μM	20mM	Ethanol
Jasplakinolide	Induces actin polymerization and stabilization	3μM	705mM	DMSO
Lantrunculin A	Inhibits actin polymerization	1μM	237mM	Ethanol

Table 1: Pharmacological agents used during experimental procedures. A brief explanation of the mechanism of action of the pharmacological agents is provided.

Abbreviation	Name
6-benzoyl-cAMP	N6-Benzoyladenosine-3',5'-cyclic monophosphate sodium salt
Forskolin	(3R, 4aR, 5S, 6S, 6aS, 10S, 10aR, 10bS)- 6, 10, 10b- trihydroxy- 3, 4a, 7, 7, 10a- pentamethyl- 1-oxo- 3- vinyldodecahydro- 1H- benzo[f] chromen-5- yl acetate
Jasplakinolide	N-[2-bromo-N-[N-(8-hydroxy-2,4,6-trimethyl-1-oxo-4-nonenyl)-L-alanyl]-N-methyl-D-tryptophyl]-L-3-(4-hydroxyphenyl)
Lantrunculin A	[1R-[1R*, 4Z, 8E, 10Z, 12S*, 15R*, 17R*(R*)]]-4-(17-Hydroxy-5,12-dimethyl-3-oxo-2,16-dioxabicyclo[13.3.1]nonadeca-4,8,10-trien-17-yl)-2-thiazolidinone
PMA	Phorbol-12-Myristate-13-Acetate; 12-O-Tetradecanoylphorbol 13-acetate, 4β,9α,12β,13α,20-Pentahydroxytiglia-1,6-dien-3-one 12-tetradecanoate
Rp-8-cpt-cAMPs	8-(4-Chlorophenylthio)adenosine-3′,5′-cyclic Monophosphorothioate, Rp-isomer sodium salt

Table 2: Abbreviations Nomenclature. An abbreviated nomenclature is provided for the pharmacological agents used during assays.

RESULTS

Effects of pharmacological agents on transfected LβT2 cells

The first set of experiments focused on rim intensity changes during confocal imaging of live imaging in LβT2 cells transfected with AKAP150-GFP. In LβT2 cells, AKAP150 protein localizes to the cell rim. The purpose of these experiments was to determine if AKAP150-GFP is mobile upon the introduction of specific pharmacological agents in solution.

Time-lapse Imaging of Transfected LβT2 Cells

The time-lapse imaging assays were performed by collecting one image every 30 seconds for approximately 10 minutes (20 time points). When collecting the live-cell data from time-lapse imaging, the change of rim brightness was plotted in a graph displaying intensity over time(s). One image was taken every 30 seconds to minimize unintended photobleaching. The experiment began with cells in the standard resting solution for two minutes (four control time points) and then switched to a resting solution with a pharmacological agent. The control cell maintained constant rim fluorescence intensity, verifying that unintended photobleaching was not causing a decrease in rim intensity. In Figures 4B-4D, where the pharmacological agents activated or inhibited PKA, the cells treated with rp8-cpt-cAMPs and forskolin showed a trend in decreasing fluorescence intensity, but the cell treated with 6-

benzoyl-cAMP did not. In Figures 4E-4F, where the pharmacological agents activated PKC and caused an increase in Ca^{+2}, the cells treated with both PMA and 100mM K^{+} showed a trend of decreasing fluorescence. Lastly, in Figures 4G-4H, where the pharmacological agents stabilized or inhibited actin polymerization, the cells treated with jasplakinolide and lantrunculin A showed a minimal decrease in fluorescence intensity. The results of experiments with PMA were promising because they indicated the translocation of AKAP150-GFP. It is possible that we did not observe a significant decrease in fluorescence intensity in the cells treated with the pharmacological agents other than PMA because AKAP150-GFP was translocating laterally. The trend in decreased fluorescence suggested possible translocation from the rim to the cytosol. Lateral translocation only of AKAP150-GFP would not cause a significant decrease in fluorescence intensity. We decided we needed a more sensitive method to study the translocation of AKAP150-GFP in anterior pituitary cells. The more sensitive method we used was FRAP.

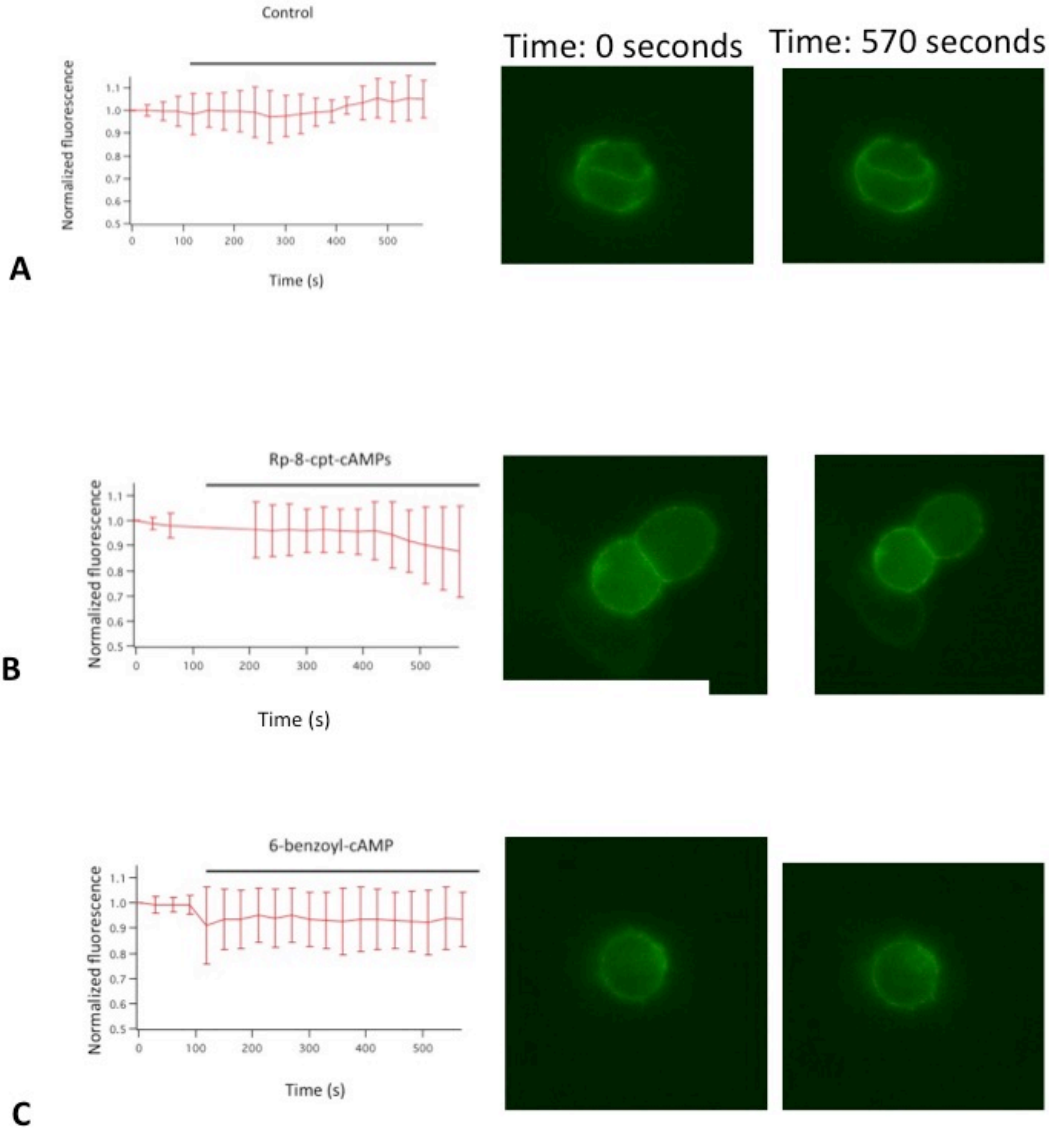
Control
Normalized fluorescence
Time (s)
Time: 0 seconds
Time: 570 seconds
A
Rp-8-cpt-cAMPs
Normalized fluorescence
Time (s)
B
6-benzoyl-cAMP
Normalized fluorescence
Time (s)
C

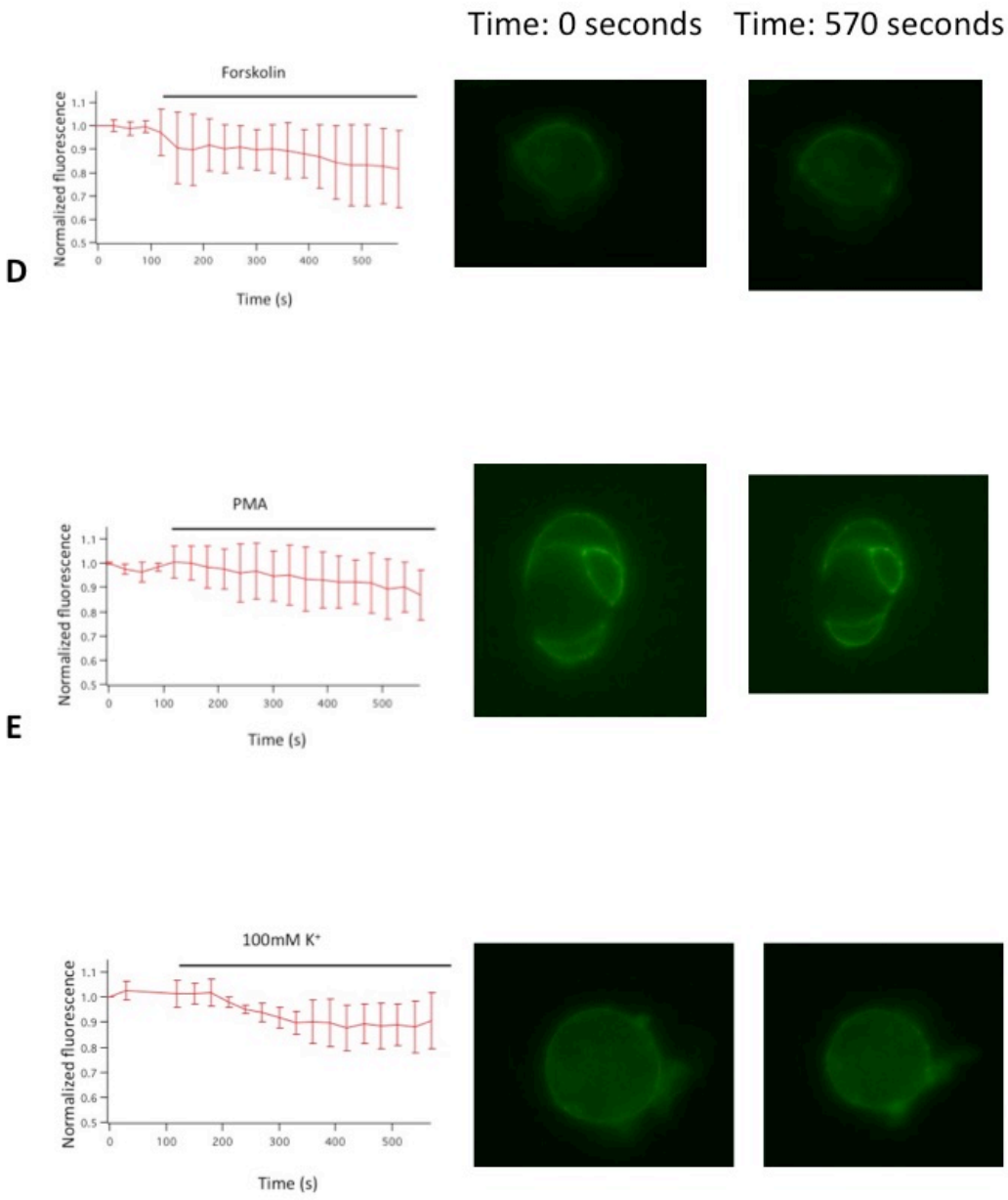
Time: 0 seconds
Time: 570 seconds
Forskolin
Normalized fluorescence
Time (s)
D
PMA
Normalized fluorescence
Time (s)
E
100mM K+
Normalized fluorescence
Time (s)
F

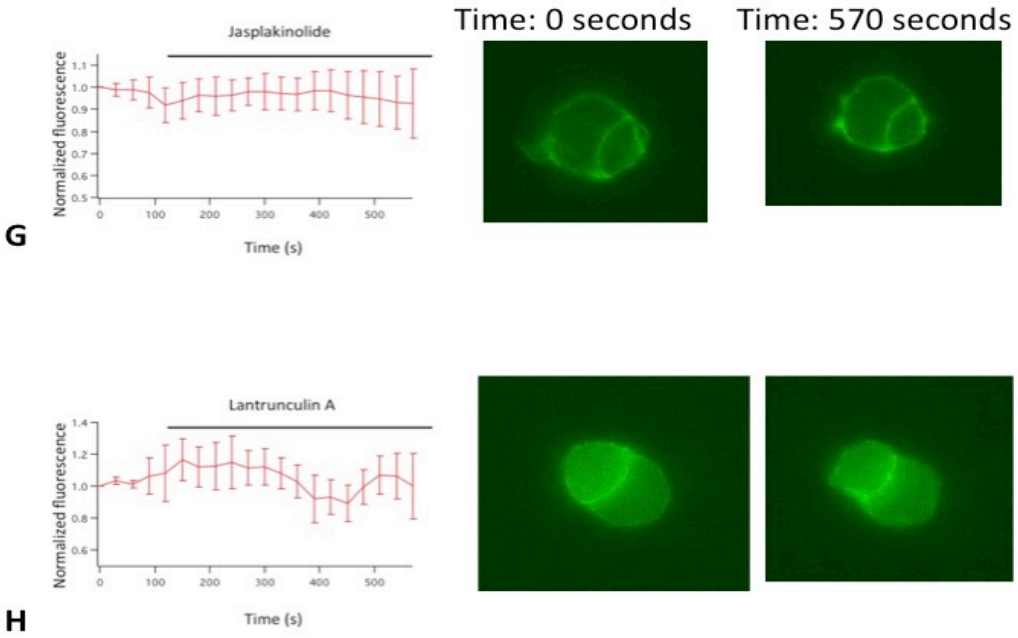

Figure 4: Mobility of AKAP150-GFP in time-lapse imaging assays. In each of the assays, LβT2 cells transfected with AKAP150-GFP were imaged once every 30 seconds for 10 minutes (20 time points). For the first two minutes (four time points), cells were bathed in standard resting solution and then switched to a resting solution containing a pharmacological agent. (A) Control (B) Rp-8-cpt-cAMPs (C) 6-benzoyl-cAMP (D) Forskolin (E) PMA (F) 100mM K+ (G) Jasplakinolide (H) Lantrunculin A

Fluorescence Recovery After Photobleaching (FRAP) on LβT2 Cells Transfected with AKAP150-GFP

To focus further on the translocation of AKAP150 in LβT2 cells, we tested the mobility of the scaffolding protein by measuring recovery of AKAP150-GFP after photobleaching. FRAP would provide a more sensitive method to test the mobility of AKAP150-GFP. It is predicted the recovery of AKAP150-GFP could translocate from the rim, cytosol or both. It is unknown how the scaffolding protein moves within the cell, for example diffusing freely or binding to a structure, such as actin. Previous in vitro studies have suggested that AKAP150 attaches directly to both the actin cytoskeleton and lipids in the membrane (Dell'Acqua et al. 2006).

Fluorescence Recovery After Photobleaching in LβT2 Cells

In order to study AKAP150-GFP mobility using a more sensitive method, we analyzed quantitative FRAP data. Baseline parameters were established for the FRAP imaging. The ROI appears to almost be completely photobleached at frame 13, which is about 3.3 seconds into the 5-second photobleach. Recovery is not apparent in the photobleached area at 5.5 seconds post-photobleach. A very dim rim is visible at 27.5 seconds post-photobleach. The rim is visible at both 159.5 and 324.5 seconds post-photobleach. Although the fluorescence of the rim recovers following photobleach, it did not appear as bright as the rim pre-photobleach. This FRAP data indicate that AKAP150-GFP in LβT2 cells is mobile.

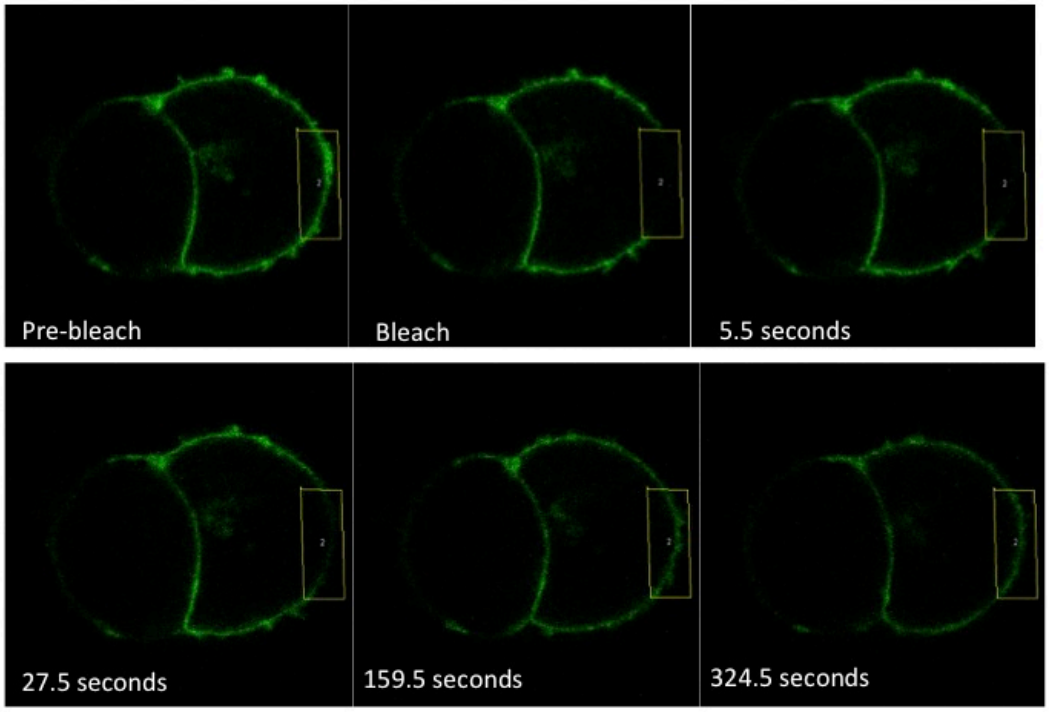

Figure 5: Fluorescence Recovery After Photobleaching (FRAP) of an LβT2 cell transfected with AKAP150-GFP. Cells were imaged on a laser scanning confocal microscope using the preliminary parameters.

Hypothetical Schematics of Recovery from FRAP

In order to visualize the origin of the recovered AKAP150-GFP in the cell, we created a post-photobleaching recovery model (Figure 7). Cell A shows the recovery of AKAP150-GFP expression originating from a cytosolic pool of AKAP150 only. Recovery from the cytosol would be considered rapid because every area along the rim that was photobleached has access to the soluble, cytosolic pool of AKAP150-GFP. Cell B shows recovery due to the lateral movement of AKAP150-GFP at the rim only. Recovery along the rim is expected to take longer because the protein must move a greater distance (laterally from the outside of the bleached area to the middle of the ROI). The green arrows above cell B show Fluorescence Loss in Photobleaching (FLIP) from the region outside of the ROI. We expect this to occur as AKAP150-GFP translocates to the inside of the ROI to aid in recovery. Cell C shows recovery of expression due to movement of AKAP150-GFP from both the rim and cytosol. Similar to Cell B, a combination of cytosolic and lateral translocation would also show FLIP in the region outside of the ROI. The difference in speeds from a combination of cytosolic and rim recoveries is dependent on the rate-limiting constant, k_{off}. K_{off} is the time it takes for a photobleached protein to detach from a subcellular structure before being replaced by a fluorescent protein from the cystolic pool or rim. Since the cytosolic pool of protein is soluble, it is predicted that recovery will occur quicker than the lateral movement of recovery along the rim. If the constants between the two recoveries are similar, it could be difficult to separate cytosolic from rim recovery. It is conceivable that a faster acquisition speed could be used to identify different recoveries.

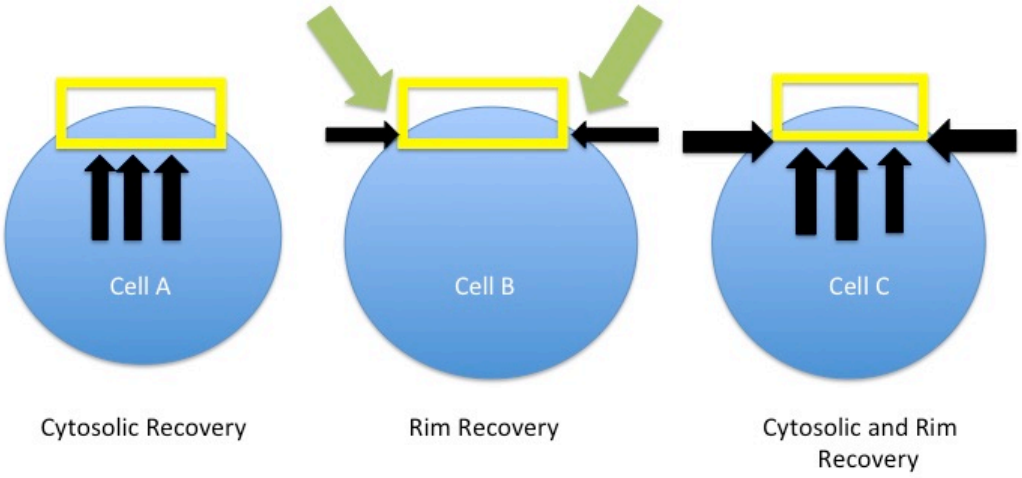

Figure 6: Model depicting lateral and cytosolic recovery of AKAP150-GFP after photobleaching. Cell A depicts cytosolic recovery of AKAP150-GFP in ROI post-photobleaching. The recovery in cell A comes from the mobile fraction of AKAP150-GFP protein found in the cytosol of LβT2 cells. Cell B depicts rim recovery of AKAP150-GFP in ROI post-photobleaching. The recovery in cell B comes from the mobile fraction of AKAP150-GFP protein found along the rim of LβT2 cells. Cell C depicts simultaneous cytosolic and rim recovery of AKAP150-GFP in ROI post-photobleaching. The recovery in cell C comes from the mobile fractions of AKAP150-GFP found in both the cytosol and rim of LβT2 cells.

Recovery Curves from LβT2 Cell after FRAP

The FRAP experiment verified the mobility of AKAP150-GFP in LβT2 cells; however, the mechanism of recovery was not understood. Thus, further analysis of the FRAP data was completed. The recovery curves in Figures 8A-8C show the recovery of fluorescence within inside of the ROI. The y-axes of the graphs represent fluorescence intensity of the AKAP150-GFP protein and the x-axes represent time. Figure 8A displays the recovery at the left edge of the ROI. Figure 8B displays the recovery in the middle of the ROI. Figure 8C displays the recovery of the right edge of the ROI. By comparing the recovery curves along the edges of the ROI to the recovery curve at the middle of the ROI, the fluorescence at the middle of the ROI takes the longest to recover. This could be due to the fact that the middle of the ROI decreases in fluorescence more than the edges. This could also result from lateral recovery of AKAP150-GFP. Figure 8D shows the intensity along the entire rim of the cell. The shape of the decrease of intensity in Figure 8D is rectangular. This is the shape that we strive to achieve each time during photobleaching because it displays consistent bleaching along the cell rim. These results demonstrate that AKAP150-GFP translocates during recovery.

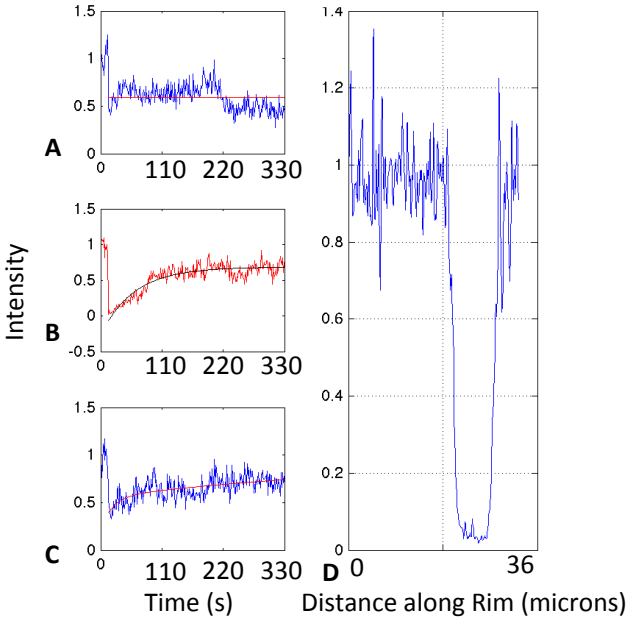

Figure 7: Recovery of AKAP150-GFP inside of the ROI using preliminary parameters during FRAP. Recovery curves were generated from the cell shown in Figure 6. The recovery curves display a change in intensity over time. (A) Change in intensity at the left edge of the ROI. (B) Change in intensity in the middle of the ROI. (C) Change in intensity at the right edge of the ROI. (D) Graph showing intensity along the entire rim of the cell.

In addition to measuring the recovery of the area inside of ROI, we examined recovery of the rim outside of the ROI. A loss in fluorescence outside of the ROI would provide the most convincing evidence that AKAP150-GFP is mobile. Figure 9A measures the change in fluorescence intensity outside of the left edge of the ROI. Figure 9B measures the change in fluorescence intensity outside of the right edge of the ROI. The gray line in Figures 9A and 9B mark when photobleaching occurred. Fluorescence Loss in Photobleaching (FLIP) occurs on both edges of the ROI. This supports the hypothesis that AKAP150-GFP translocates laterally from the outside of the ROI to the inside of the ROI during recovery after photobleaching.

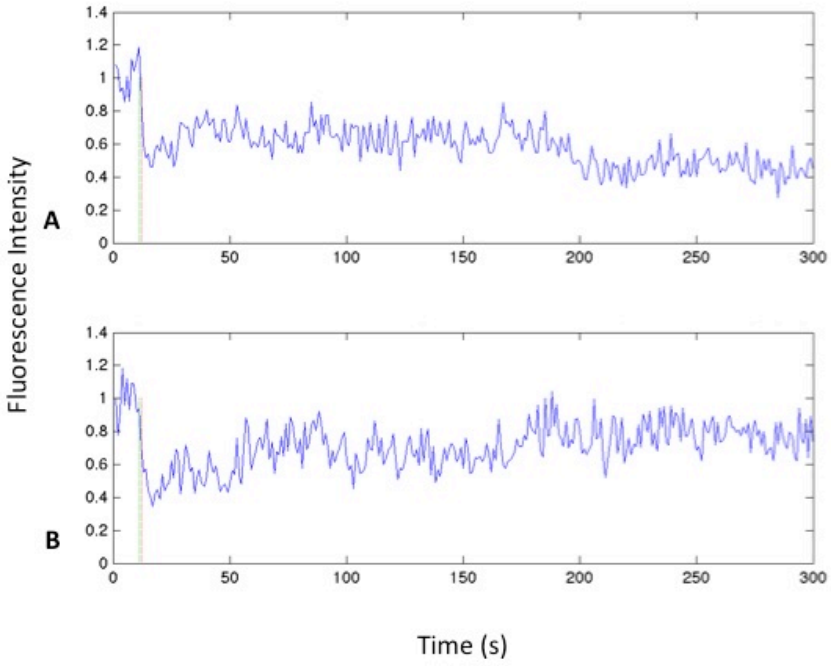

Figure 8: Fluorescence Loss in Photobleaching (FLIP) in the rim outside of the ROI. Preliminary parameters were used for imaging during FRAP. An area of 0.5 microns was measured on each side along the rim outside of the ROI. Recovery curves were generated from the cell shown in Figure 6. The recovery curves display the change in intensity over time. (A) Change in intensity at the left edge outside of the ROI. (B) Change in intensity at the right edge outside the ROI.

Simulation Heat Maps of Recovery from FRAP

Simulation heat maps were created to depict changes in fluorescence intensity along the cell rim over time (Figure 10). The simulated data in the heat maps demonstrate predicted data. The heat maps show relative intensity of the cell rim over time. The color red depicts a high intensity, or maximum fluorescence, with a value of 1. The color blue depicts a low intensity, or zero fluorescence, with a value of 0. The x-axis of the heat map represents the cell membrane. The y-axis of the heat map represents time. The black bars on the heat map show the boundaries of the ROI. The heat map in Figure 10A shows the fluorescence recovery if AKAP150-GFP recovered only from the cytosol. The cytosolic recovery appears to have a flat base since the rate recovery should be the same along the entire distance of the rim. The heat map in Figure 10B is the predicted recovery if AKAP150-GFP recovered laterally along the rim. The shape of the signal is more ovoid and demonstrates that the middle of the bleached region is the last to recover. The heat map in Figure 10C is the hypothetical recovery if AKAP150-GFP were to recover from both the cytosol and cell rim. A combination of lateral and cytosolic recovery creates wing-like shapes during FLIP outside of the ROI.

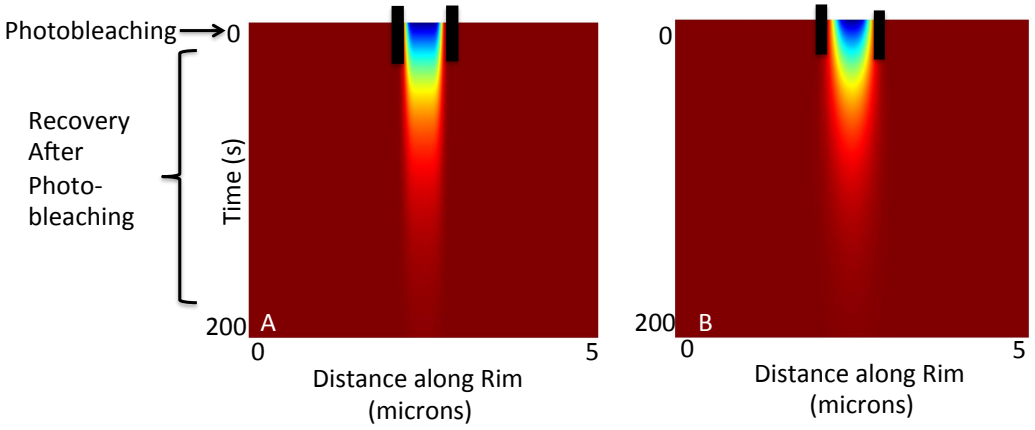

Figure 9: Simulation heat maps of AKAP150-GFP recovery after FRAP. The x-axis displays distance along the membrane. The y-axis displays time. The color red indicates a high intensity, or the maximum fluorescence. The color blue indicates a low intensity, or zero fluorescence. The black bars represent the boundary of photobleaching. The heat map demonstrates (A) Recovery from cytosol. (B) Lateral recovery from the rim.

Heat Map of LβT2 Cell Recovery after FRAP

A heat map depicting the recovery of AKAP150-GFP from FRAP data was plotted to determine if recovery was occurring from the cytosol, rim or both (Figure 11). The x-axis represents the distance along the rim of the cell, and the y-axis represents time. The two arrows at the top of the heat map indicate the boundaries of the ROI. The red color at the top of the membrane depicts the first 11 seconds of the imaging before bleaching occurred. The deep blue color after the red portion depicts the 5-second bleach. The rest of the image after the 5-second bleach shows the recovery of the cell 314 seconds (5.2 minutes). Immediately after the cell was bleached for 5 seconds, the ROI decreases in fluorescence intensity and remains at a decreased intensity over time. The fluorescence loss in photobleaching outside of the ROI indicates that AKAP150-GFP translocates from outside of the ROI to inside of the ROI. This result further supports what we observed Figure 8 and Figure 9. Together, these results strongly suggest that AKAP150-GFP translocates laterally after photobleaching.

While analyzing the heat maps, we noticed spots along the rim (relatively distant from the ROI) that changed in fluorescence over time. The spots showed dynamic changes in fluorescence on a much slower time scale than FRAP. We thought that the spots could be the result of over expression of the AKAP150-GFP plasmid. Due to this, we focused on improving temporal resolution rather than investigating the nature of the spots.

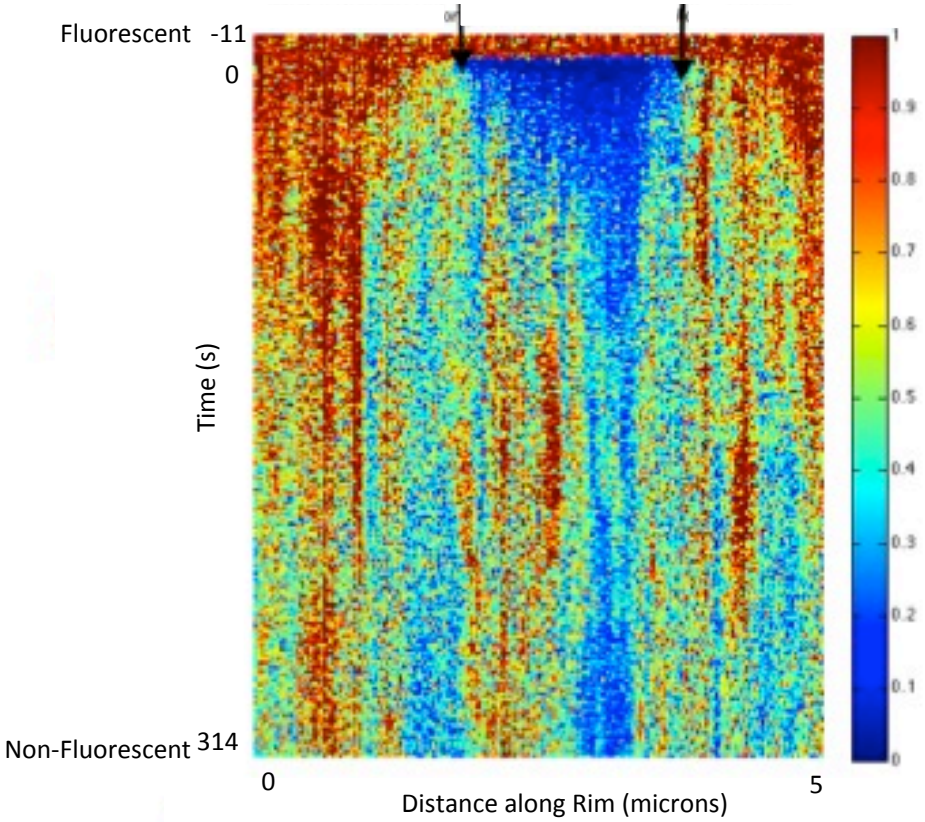

Figure 10: Heat map displaying AKAP150-GFP recovery using preliminary parameters during FRAP. The preliminary parameters were used for imaging during FRAP. The x-axis is distance along the membrane. The y-axis is time. The black arrows indicate the boundaries of the ROI. Red is fluorescent. Blue is non-fluorescent.

Method Development

Rapid Photobleaching with Rectangular Regions of Interest

Since concluding that AKAP150-GFP is mobile in LβT2 cells, we wanted to maximize the capabilities of the confocal microscope to ascertain if we could differentiate between cytosolic and rim recoveries. We determined that a faster acquisition speed and decreased photobleach duration were needed in order to detect differences between lateral and cytosolic recovery during the fast phases of recovery. Since we predicted that recovery from the cytosol is rapid due to availability of soluble protein, it was important to bleach for as little time as possible so as to not bleach the proteins potentially aiding in recovery. In addition to increasing acquisition speed, we found that a decreased aspect ratio binned pixels in a smaller area, allowing for a quicker frame rate. Using these new parameters, we analyzed recovery with the fast rectangle parameters. We continued to use a rectangular ROI because it did not bleach as far into the cytosol as a circular ROI.

Two different photobleach time spans were used to examine recovery of AKAP150-GFP during FRAP with the fast rectangle parameters. One photobleach time span lasted 1 second. The other photobleach time span lasted 2.5 seconds. The ROI drawn around the cell in the different time spans was the same size and positioned vertically around the rim of one cell, as shown in Figure 6. When comparing bleach time spans at 1 second, it was noticed that there was a lot of variability in the extent of ROI was photobleaching (Figures 12A and 12B). The same trend was noticed when comparing the 2.5 second bleach time spans (Figures 12C and 12D). In Figure 12B, photobleaching for one second decreased

fluorescence intensity to near zero along the entire length of the ROI. The shape of the region photobleached appears as a rectangle. This is different from Figure 12A, where photobleaching with the same settings neither decreased fluorescence intensity to the same degree nor photobleached in the shape of a rectangle. The same trend of variation in shape and decreased fluorescence intensity was observed in Figures 12C and 12D, where the cells were photobleached for 2.5 seconds.

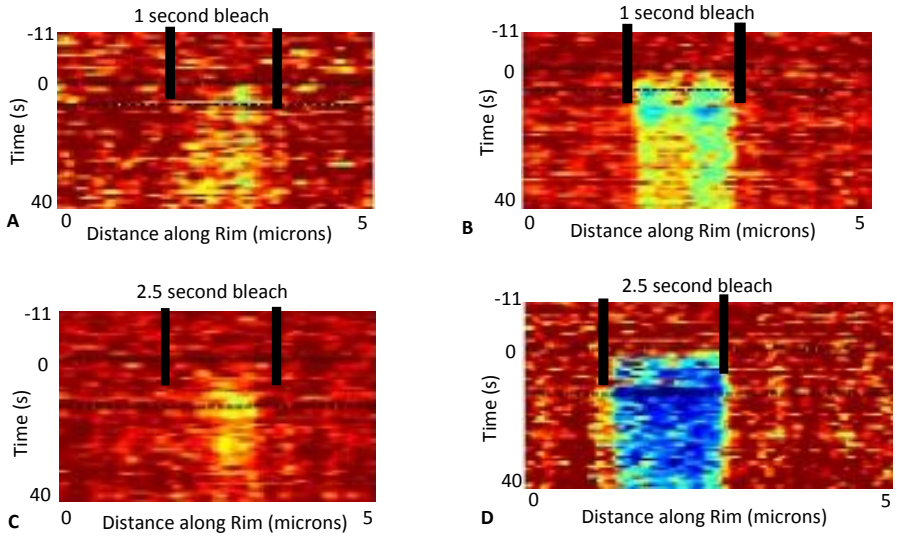

Figure 11: Comparison of ROIs when using fast rectangle parameters during FRAP. (A) Cell photobleached for one second. (B) Cell photobleached for one second. (C) Cell photobleached for 2.5 seconds. (D) Cell photobleached for 2.5 seconds.

In the process of method development, we treated cells with Rp-8-cpt-cAMPs to potentially determine a biological effect of inhibiting protein kinase A. Figure 13 measures recovery of a control cell photobleached for one second. Figure 14 measures recovery of a cell treated with rp-8-cpt-cAMPs and photobleached for one second. The fast rectangle parameters were used when imaging these cells. When comparing the recovery of the control cell to the drug treated cell after one second of photobleaching, it is difficult to perceive a difference. The recovery curves at the edges of the ROI in the control cell recovered instantly (Figures 13A and 13C) whereas the recovery curves at the edges of ROI in the rp-8-cpt-cAMPs treated cell took more time to recovery (Figures 14A and 14C). Recovery in the middle of the ROI in control cell (Figure 13B) was quicker than in the cell treated with rp-8-cpt-cAMPs (Figure 14B). The photobleaching decreased fluorescence shape of a rectangle in the cell treated with rp-8-cpt-cAMPs (Figure 14D), but not in the control cell (Figure 13D). This could account for the difference in appearance of the recovery curves. The heat maps also show the difference of the photobleaching between the control (Figure 13E) and cell treated with rp-8-cpt-cAMPs (Figure 14E). The difference in photobleaching could account for the differences in recovery. It is not yet possible to determine if the difference in recovery was from treatment with rp-8cpt-cAMPs. Due to the variability of photobleaching within the ROIs of the control and drug-treated cells, it was difficult to interpret the biological significance of the results.

Considering that the results with a one second photobleach were difficult to interpret, we decided to compromise speed for greater bleach efficacy. Figure 15

measures recovery of a control cell photobleached for 2.5 seconds. Figure 16 measures recovery of a cell treated with rp-8-cpt-cAMPs and photobleached for 2.5 seconds. Both cells were imaged using the fast rectangle parameters during FRAP. The recovery of the fluorescence of the cell treated with rp-8-cpt-cAMPs (Figure 16) was different from that of the control cell (Figure 15). The recovery curves for the outside edges of the ROI in the control cell recover quicker and to pre-bleach fluorescence intensity (Figures 15A and 15C). The recovery curves for the outside edges of the ROI in the cell treated with rp-8-cpt-cAMPs show a slower increase in fluorescence and do not appear to recover to the pre-bleach fluorescence intensity (Figures 16A and 16C). These same trends were observed in the heat maps (Figures 15E and 16E). In both of the heat maps, a small amount of FLIP is observed outside of the ROI, indicating lateral recovery. Similar to the cells photobleached for one second using a rectangular ROI, a lot of variability occurred in the photobleaching with a 2.5-second time span. The decrease in fluorescence intensity during photobleaching is not as uniform in the control cell (Figure 15D) as the cell treated with rp-8-cpt-cAMPs (Figure 16D). Due to this variability, we could not come to any biological conclusions about the effects of treatment with rp-8-cpt-cAMPs. We did conclude that photobleaching for 2.5 seconds produces a consistent decrease in fluorescence intensity in the ROI.

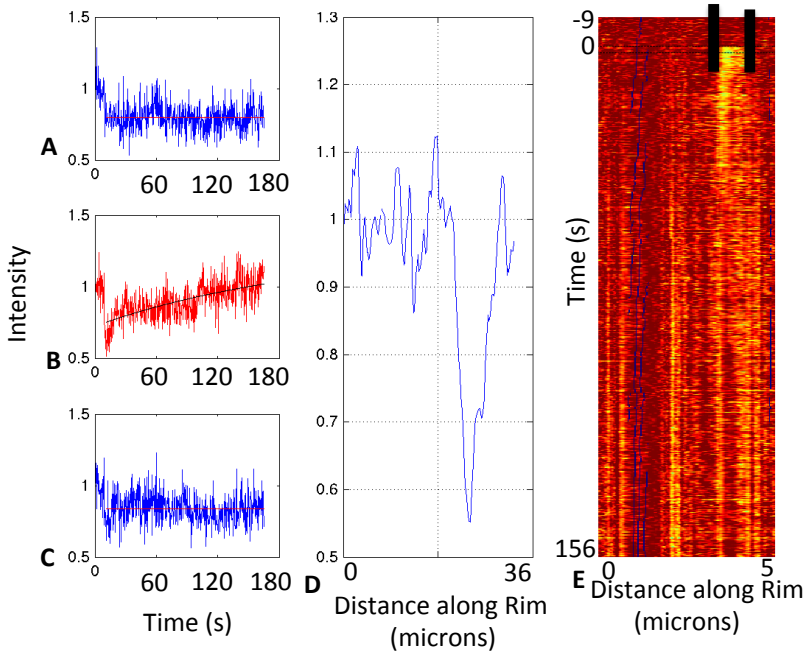

Figure 12: Recovery of AKAP150-GFP after photobleaching for one second using the fast rectangle parameters. (A) Change in intensity at the left edge of the ROI. (B) Change in intensity in the middle of the ROI. (C) Change in intensity at the right edge of the ROI. (D) Fluorescence intensity along the entire rim of the cell. (E) Heat map after FRAP. The black bars show the boundaries of the ROI.

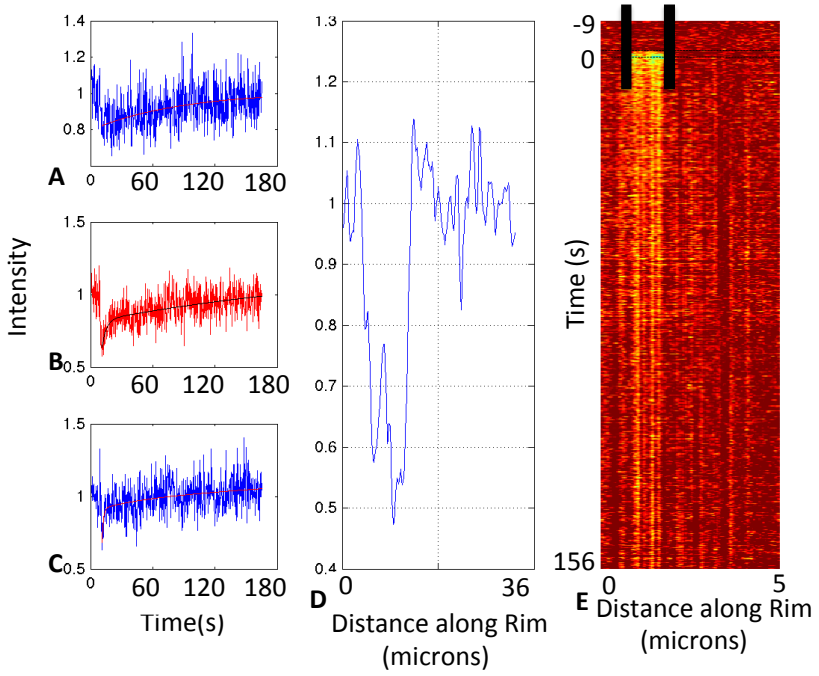

Figure 13: Recovery of AKAP150-GFP treated with rp-8-cpt-cAMPs after photobleaching for one second using the fast rectangle parameters. (A) Change in intensity at the left edge of the ROI. (B) Change in intensity in the middle of the ROI. (C) Change in intensity at the right edge of the ROI. (D) Fluorescence intensity along the entire rim of the cell. (E) Heat map after FRAP. The black bars show the boundaries of the ROI.

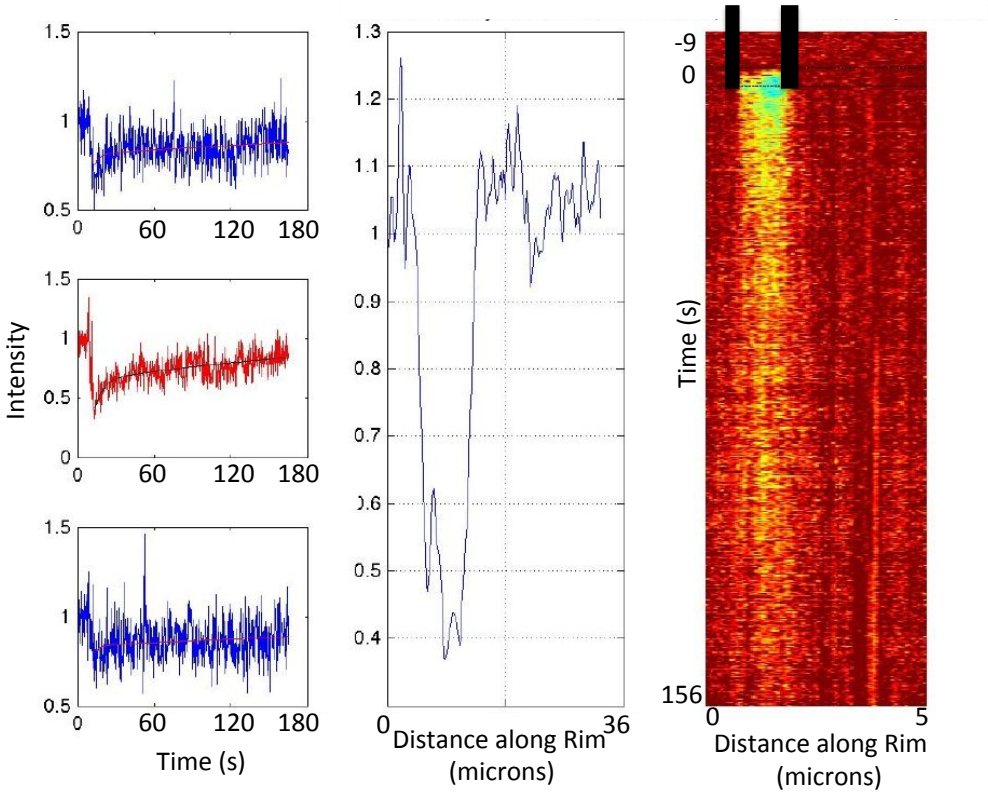

Figure 14: Recovery of AKAP150-GFP after photobleaching for 2.5 seconds using the fast rectangle parameters. (A) Change in intensity at the left edge of the ROI. (B) Change in intensity in the middle of the ROI. (C) Change in intensity at the right edge of the ROI. (D) Fluorescence intensity along the entire rim of the cell. (E) Heat map after FRAP. The black bars show the boundaries of the ROI.

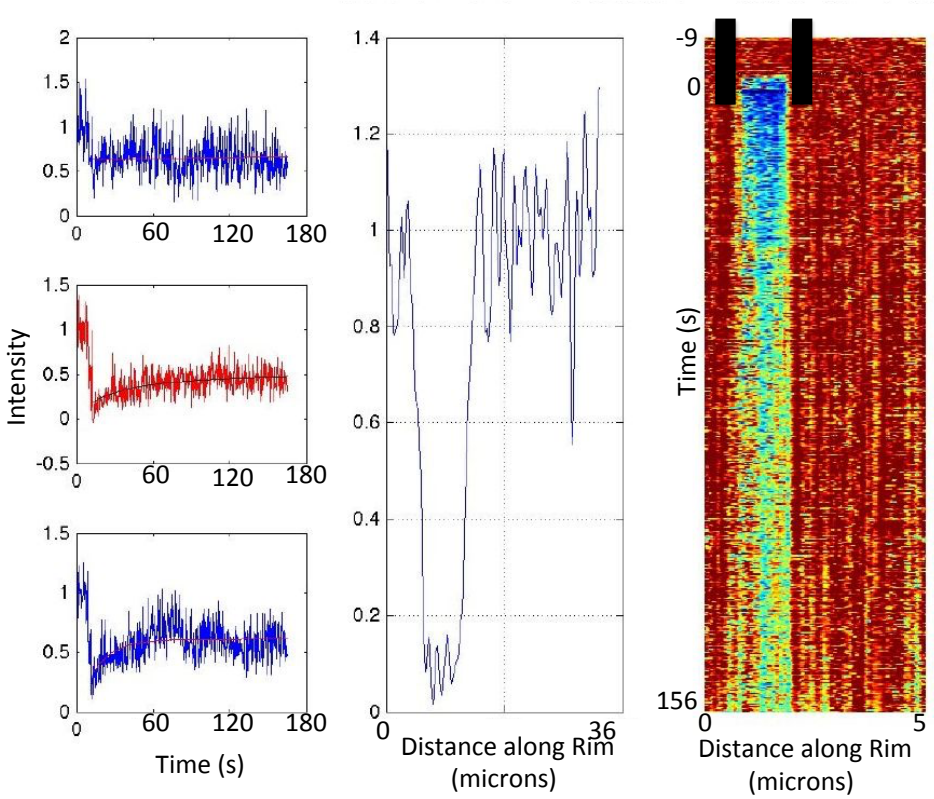

Figure 15: Recovery of AKAP150-GFP treated with rp-8-cpt-cAMPs after photobleaching for 2.5 seconds using the fast rectangle parameters. (A) Change in intensity at the left edge of the ROI. (B) Change in intensity in the middle of the ROI. (C) Change in intensity at the right edge of the ROI. (D) Fluorescence intensity along the entire rim of the cell. (E) Heat map after FRAP. The black bars show the boundaries of the ROI.

Rapid Photobleaching with Tornado Region of Interest

Since using a rectangular region of interest did not provide homogenous photobleaching within the ROI, we photobleached more of the cytosol in order to achieve more consistent results. The tool we used to provide a more consistent photobleach was the tornado ROI; the settings used during these experiments are referred to as fast tornado parameters. Similar to the data collected when using the rectangular ROI, cells were photobleached for either one second or 2.5 seconds. The shape of the tornado ROI was the same size in each of the movies and the location of the ROI on each of the cell rims was similar. Figure 17 measures recovery of a control cell after one second of photobleaching. Figure 18 measures recovery of a cell treated with rp-8-cpt-cAMPs after one second of photobleaching. The decrease in fluorescence intensity due to photobleaching is less in the control cell (Figure 17D) than in the cell treated with rp-8-cpt-cAMPs. The recovery curves of the edges and middle of the ROI in the control cell look very different from the cell treated with rp-8-cpt-cAMPs. In the recovery curve for the left edge of the ROI, recovery occurs very quickly and then decreases again. The same trend is observed in recoveries at the right edge and at the middle of the ROI (Figure 17B and 17C). The recovery curve of the left edge of the ROI in the cell treated with rp-8-cpt-cAMPs does not appear to decrease in fluorescence intensity, indicating that it was never photobleached or recovered as it was photobleached (Figure 18A). The recovery curves of the right edge and middle of the ROI show the same trends (Figure 18C and 18B). The recovery curve showing the middle of the ROI in the cell treated with rp-8-cpt-cAMPs decreases in fluorescence intensity for a longer time than the right edge

of the ROI, but then appears to recover quicker (Figure 18D). However, in the heat map of the control cell (Figure 17E), FLIP outside of the ROI is not observed, making it difficult to come to a conclusion about the translocation of AKAP150-GFP. In the heat map from the cell treated with rp-8-cpt-cAMPs, (Figure 18E), FLIP does occur outside of the ROI, indicating lateral movement of AKAP150-GFP. Similar to the data collected with the fast rectangle parameters, we could not come to any biological conclusions about the recovery of AKAP150-GFP due to the inconsistency of photobleaching. Thus, we decided to compromise speed for greater photobleach efficacy. Figure 19 shows recovery of a control cell photobleached for 2.5 seconds. Figure 20 shows recovery of a cell treated with rp-8-cpt-cAMPs and photobleached for 2.5 seconds. When comparing the recoveries, it is difficult to determine if there is a biological difference with treatment of rp-8-cpt-cAMPs. The difference could be from inconsistent photobleaching. The decrease of fluorescence intensity during photobleaching in the cell treated with rp-8-cpt-cAMPs (Figure 20D) is greater than in the control cell (Figure 19D). Recovery is slowest in the middle of the ROI in the control cells, indicating lateral translocation of AKAP150-GFP (Figure 19B). Recovery in the cell treated with rp-8-cpt-cAMPs is slower than in the control cell. Recovery in the middle of this ROI was the slowest and never recovered to pre-bleach fluorescence intensity (Figure 20C). The differences in fluorescence intensity during photobleaching were also observed in the heat maps. In the cell treated with rp-8-cpt-cAMPs, the ROI is blue, indicating complete photobleaching of the ROI. This was not observed in the control cell. Due to the variability of photobleaching, we are not yet able to come to a conclusion about the recovery of AKAP150-GFP in cells treated

with rp-8-cpt-cAMPs. Similar to the rectangular ROI, photobleaching for 2.5 seconds with the tornado ROI produced promising results for future experiments.

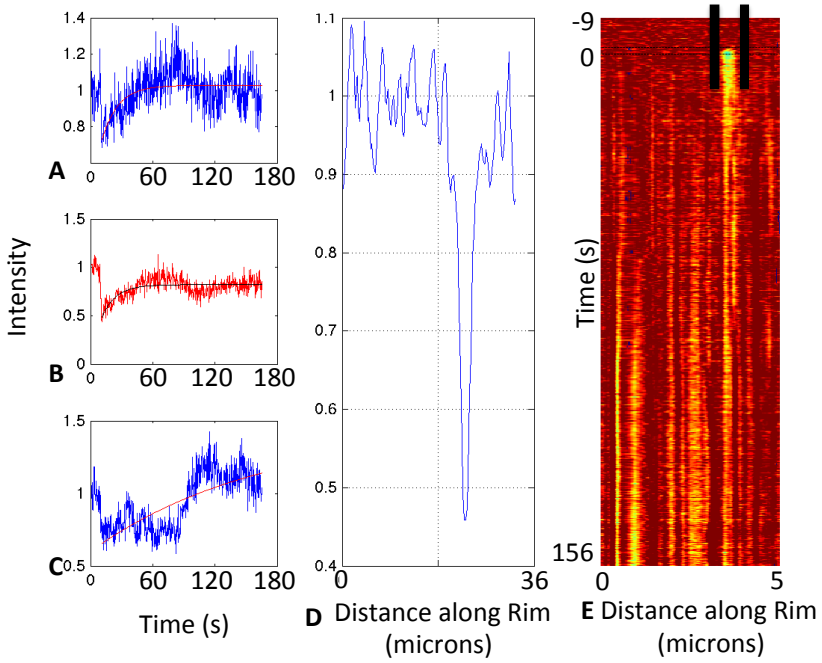

Figure 16: Recovery of AKAP150-GFP after photobleaching for one second using the fast tornado parameters. (A) Change in intensity at the left edge of the ROI. (B) Changes in intensity in the middle of the ROI. (C) Changes in intensity at the right edge of the ROI. (D) Fluorescence intensity along the entire rim of the cell. (E) Heat map after FRAP. The black bars show the boundaries of the ROI.

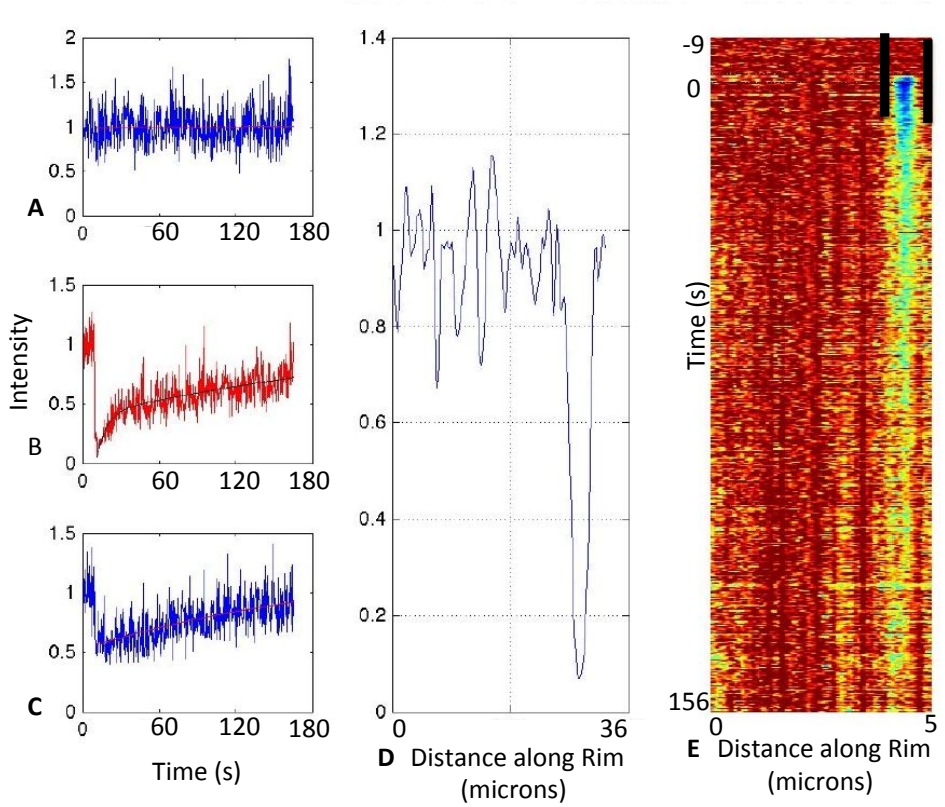

Figure 17: Recovery of AKAP150-GFP treated with rp-8-cpt-cAMPs after photobleaching for one second with the fast tornado parameters. (A) Changes in intensity at the left edge of the ROI. (B) Changes in intensity in the middle of the ROI. (C) Changes intensity at the right edge of the ROI. (D) Changes intensity along the entire rim of the cell. (E) Heat map after FRAP. The black bars show the boundaries of the ROI.

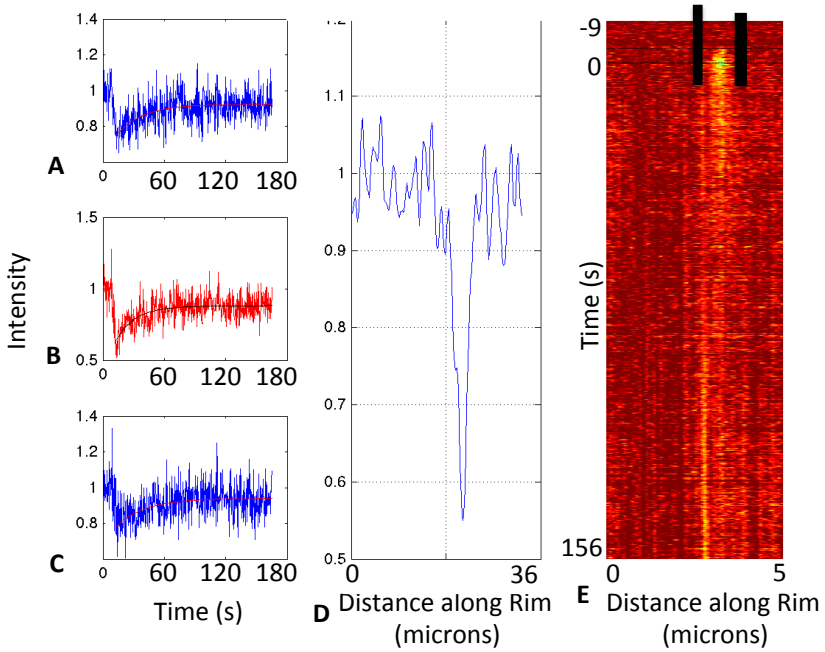

Figure 18: Recovery of AKAP150-GFP after photobleaching for 2.5 seconds using the fast tornado parameters. (A) Changes in intensity at the left edge of the ROI. (B) Changes in intensity in the middle of the ROI. (C) Changes in intensity at the right edge of the ROI. (D) Fluorescence intensity along the entire rim of the cell. (E) Heat map after FRAP. The black bars show the boundaries of the ROI.

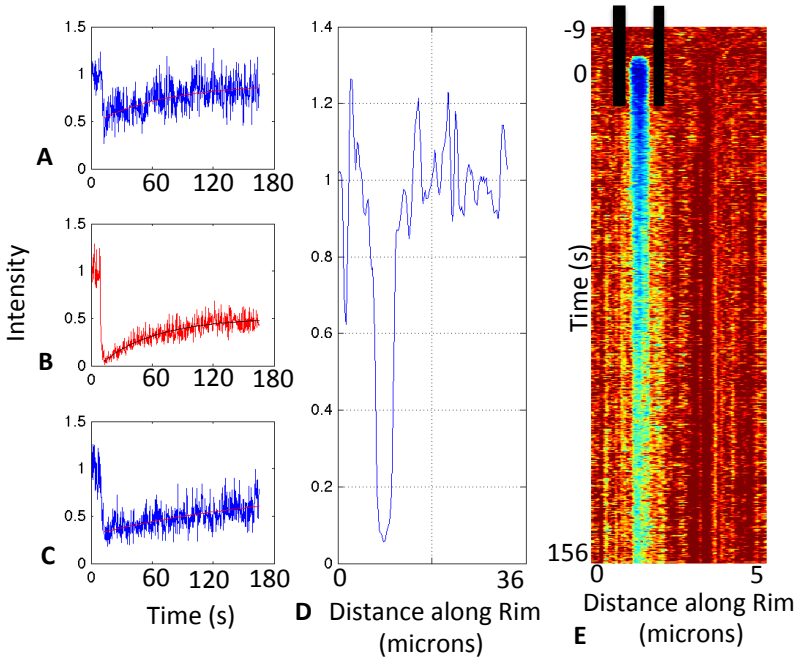

Figure 19: Recovery of AKAP150-GFP after treated with rp-8-cpt-cAMPs and photobleaching for 2.5 seconds using the fast tornado parameters. (A) Changes in intensity at the left edge of the ROI. (B) Changes in intensity in the middle of the ROI. (C) Changes in intensity at the right edge of the ROI. (D) Fluorescence intensity along the entire rim of the cell. (E) Heat map after FRAP. The black bars show the boundaries of the ROI.

Since the extent of photobleaching showed substantial variability, we compared the intensity profiles of the tornado ROIs (Figure 21) to verify that the decrease in fluorescence intensity produced by each ROI was different. In theory, the decrease in fluorescence intensity from photobleaching for 2.5 seconds should be greater than photobleaching for one second. The size of each ROI in Figure 21 is the same with the exception of the ROI represented by the red profile. This ROI represented by the red profile was slightly smaller. The decrease in fluorescence intensity was not uniform when photobleaching for either one second or 2.5 seconds. Under the same conditions, photobleaching for one second or 2.5 seconds yields the same decrease in fluorescence intensity. Photobleaching for the same amount of time yields different decreases in fluorescence intensity. The two profiles with the largest decrease fluorescence intensity were photobleached for different times; one was photobleached for one second and the other photobleached for the 2.5 seconds. The shape created by the decrease in fluorescence intensity shown with the ROIs represented by the red and black profiles was what we aimed to achieve during each photobleach. We are now aware we can achieve this shape, but are unsure of how to consistently achieve it.

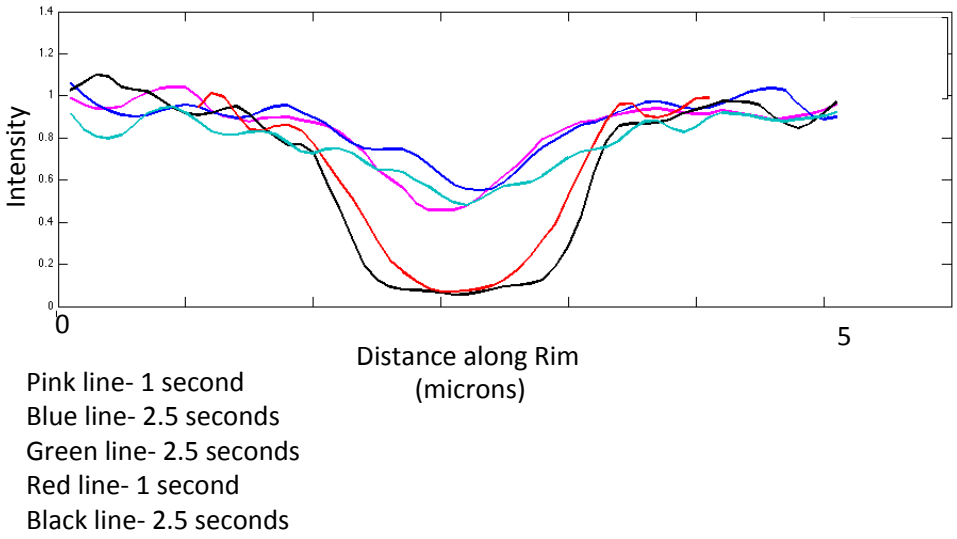

Figure 20: Comparison of intensity profiles during photobleaching using the fast tornado parameters. The size of the ROI was the same in each profile with the exception of the ROI designated by the red line, which used a slightly smaller ROI. The profiles labeled as Control are control cells. Profiles labeled as Drug are cells treated with rp-8-cpt-cAMPs. Control 9 was photobleached for one second. Control 10, was photobleached for 2.5 seconds. Drug 10 was photobleached for 2.5 seconds. Drug 11 was photobleached for one second. Drug 12 was photobleached for 2.5 seconds.

Immunostaining of Endogenous AKAP150 and Actin

To determine if the spots were a result of over expression of AKAP150-GFP, control LβT2 cells were immunostained for endogenous AKAP150 and actin (Figure 23). Endogenous AKAP150 staining revealed a rim composed of spots, verifying that the spots are not a result of over expression. Cells immunostained with endogenous AKAP150 were treated with rp-8-cpt-cAMPs or 6-benzoyl-cAMP. When comparing rim brightness in the control, rp-8-cpt-cAMPs-treated and 6-benzoyl-cAMP-treated cells, it is difficult to identify a differnce. When comparing the rim brightness of actin in the control, rp-8-cpt-cAMPs-treated and 6-benzoyl-cAMP-treated cells, the actin treated with rp-8-cpt-cAMPs appears brightest. We did not make any intensity measurements on the spots. The appearance of increased brightness was determined by how they appeared to us. There is a similarity between the bright spots on the cells immunostained for AKAP150 and actin, suggesting that AKAP150 and actin are localized in the same areas.

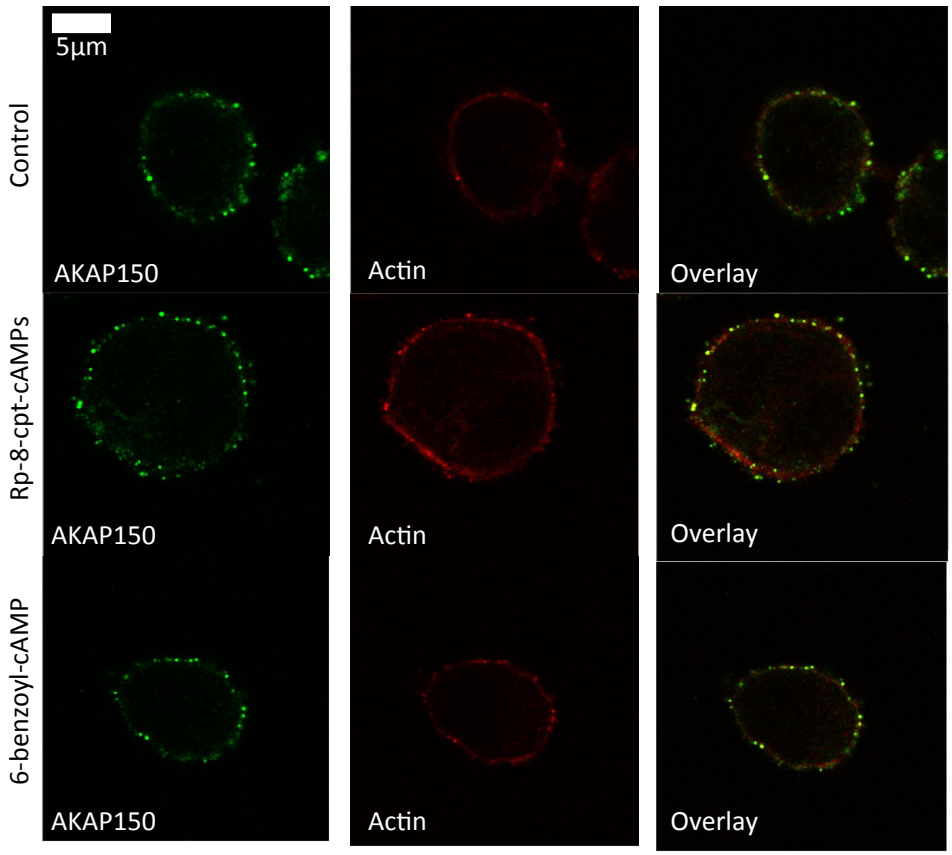

Figure 21: Immunostaining of endogenous AKAP150 and actin. Cells were fixed, permeabilized and immunostained for AKAP150 and actin. Cells were imaged using a laser scanning confocal microscope. AKAP150 was imaged with the Alexa 488 laser with 5% transmission. Actin was imaged with the Alexa 568 laser set to 5% transmission.

To analyze whether there was a statistically significant difference in fluorescence intensity between control cells and cells treated with rp-8-cpt-cAMPs and 6-benzoyl-cAMP, a students's t-test was used. In addition to the t-test, dot plot graphs were created to demonstrate the normal distribution and median of fluorescence intensity (Figure 24). There is a significant difference in AKAP150 fluorescence intensity between the control cells and the cells treated with rp-8-cpt-cAMPs. There is also a significant difference in AKAP150 fluorescence intensity between the control cells and the cells treated with 6-benzoyl-cAMP. In both results, AKAP150 decreased fluorescence intensity after treatment with the pharmacological agent. It was not the same case with actin. There is a significant difference in actin fluorescence intensity between control cells and cells treated with 6-benzoyl-cAMP, but not in cells treated with rp-8-cpt-cAMPs.

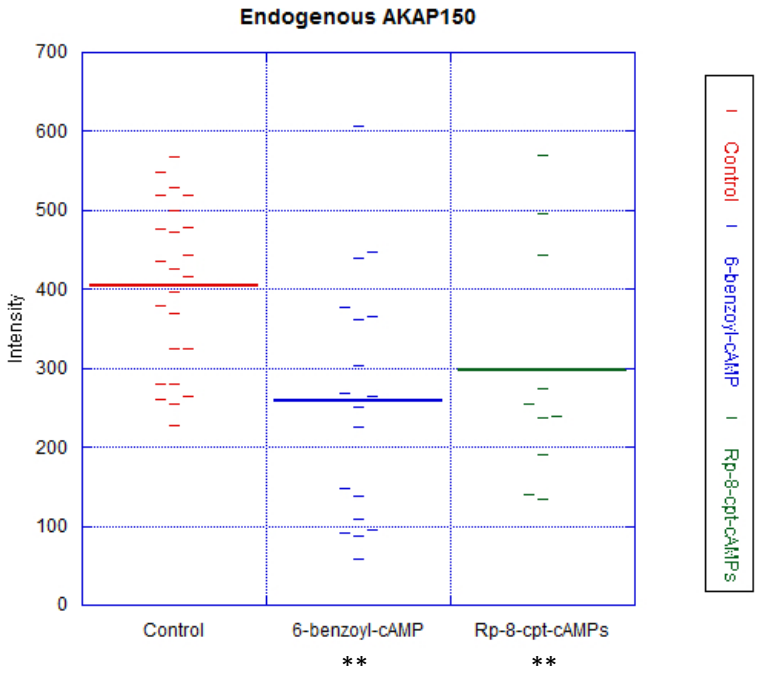

Figure 22: Comparison endogenous AKAP150 rim brightness in cells treated with rp-8-cpt-cAMPs or 6-benzoyl-cAMP. Cells were imaged on a scanning laser confocal microscope. Control cells N= 24, Cells treated with rp-8-cpt-cAMPs N=10, Cells treated with 6-benzoyl-cAMP N=18. Cells were imaged using the same settings as the endogenous staining. Statistics: Student t-test between control cells and cells treated with rp-8-cpt-cAMPs, p=0.025. Student t-test between control cells and cells treated with 6-benzoyl-cAMP, p=0.0007.

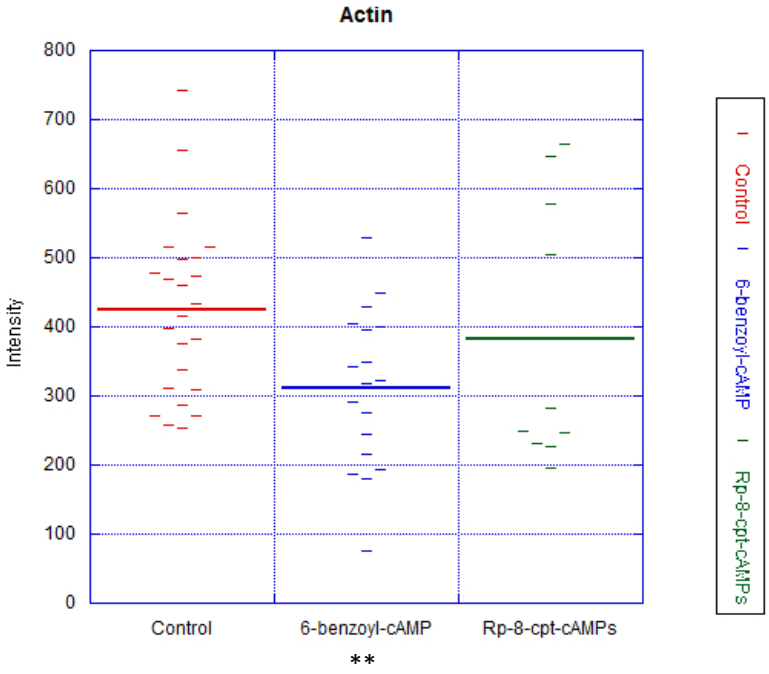

Figure 23: Comparison of actin rim brightness in cells treated with rp-8-cpt-cAMPs or 6-benzoyl-cAMP. Cells were imaged on a scanning laser confocal microscope. Cells were analyzing by drawing masks on the fluorescent rims and subtracting background. Control cells N= 24, Cells treated with rp-8-cpt-cAMPs=10, Cells treated with 6-benzoyl-cAMP N=18. Cells were imaged using the same settings as the endogenous staining. Statistics: Student t-test between control cells and cells treated with rp-8-cpt-cAMPs, p=0.464. Student t-test between control cells and cells treated with 6-benzoyl-cAMP, p=0.005.

Permeabilization Assay in Transfected LβT2 Cells

Seeing that the rims of the LβT2 cells stained for endogenous AKAP150 had a more puncta appearance than the cells transfected with AKAP150-GFP, we wondered if permeabilization was causing AKAP150 to disappear. If AKAP150 was binding to lipids in the cell membrane, it is possible that the holes created by Triton X-100 during permeabilization were causing AKAP150 to leave the rim. Cells were permeabilized after fixation, but before the addition of DAPI. Images of cells permeabilized or non-permeabilized were compared to demonstrate differences in rim appearance (Figure 25). The cells in Figure 25A had intact rims and the cells in Figure 25B were permeabilized. There was a difference in the appearance of the rim when comparing the intact to the permeabilized cell rim. The rim of the cell permeabilized exhibits a slight increase in puncta appearance, but it does not look similar to endogenous rim staining of AKAP150. The changes in fluorescence intensity were compared using a dot plot illustrating the distribution and median of the data (Figure 26). While there was a significant statistical difference in rim brightness, the non-normal distribution is mostly likely caused by transient nature of transfection. Each cell does not over-express the same amount of AKAP150-GFP during a transfection, leading to a non-normal distribution of fluorescence intensity. Based on these results, we concluded that the AKAP150 endogenous staining pattern in LβT2 cells was substantive.

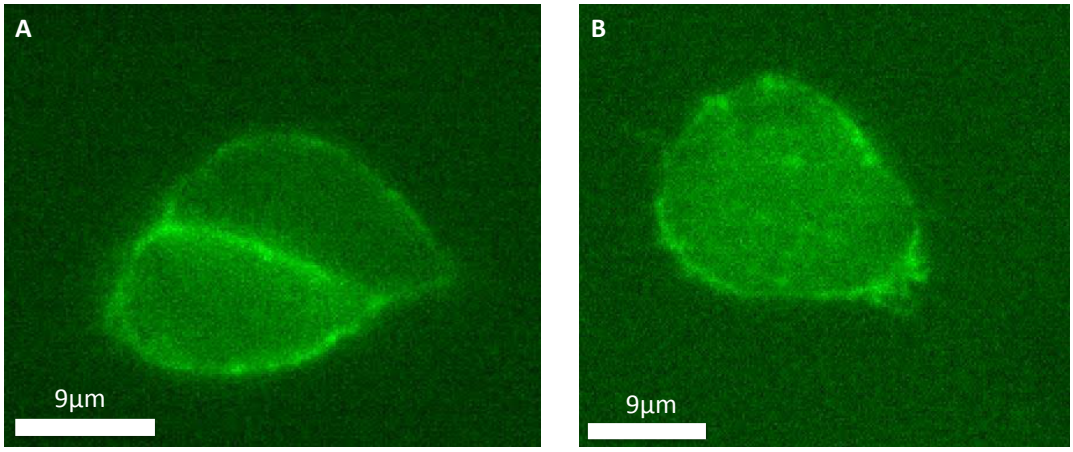

Figure 24: Comparison of rims from intact and permeabilized LβT2 cells transfected with AKAP150-GFP. Non-permeabilized (intact) cells were fixed after transfection with AKAP150-GFP. Permeabilized cells treated with Triton X-100 before fixation.

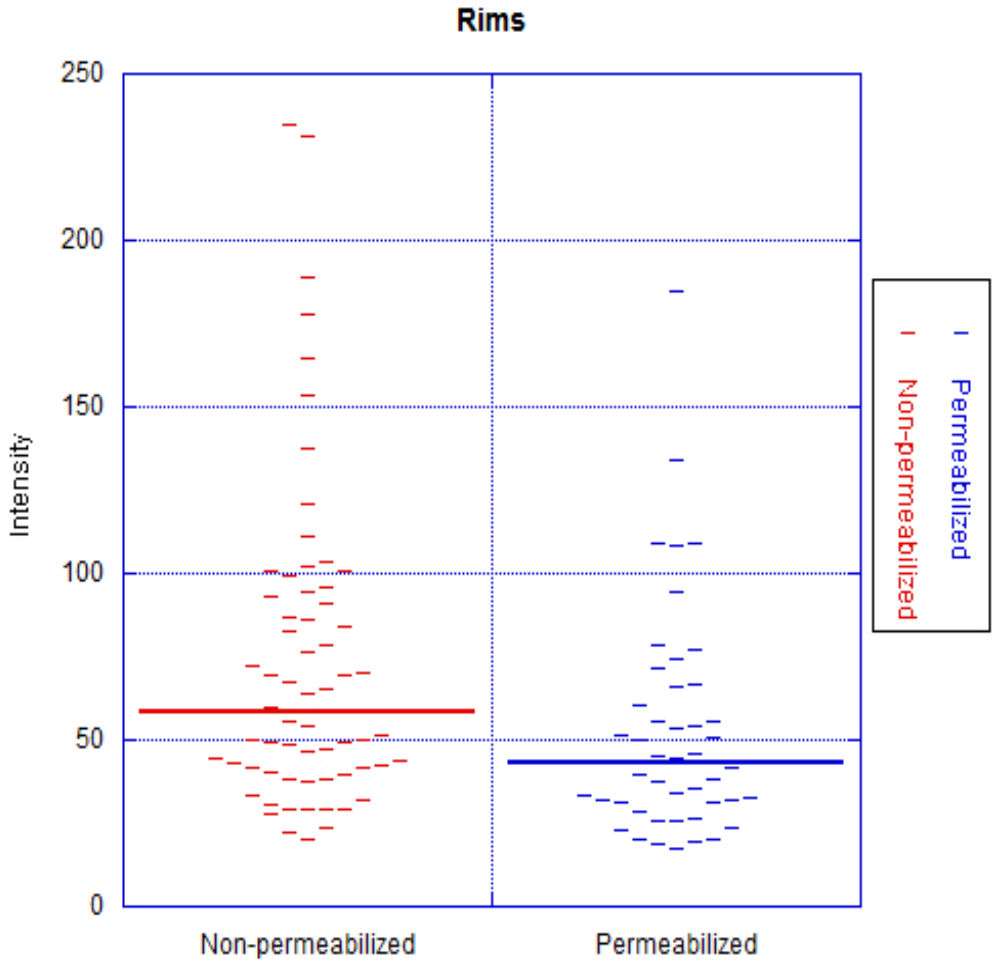

Figure 25: Comparison of rim brightness from intact and permeabilized LβT2 cells transfected with AKAP150-GFP. Non-permeabilized (intact) cells were fixed after transfection with AKAP150-GFP. Permeabilized cells treated with Triton X-100 before fixation. Non-permeabilized cells: N=65, median intensity: 58.472. Permeabilized cells: N=46, median intensity: 42.987. Statistics: Wilcoxon-Rank-Sum Test, p=0.006.

DISCUSSION

Major Conclusions

From our experiments we conclude that AKAP150-GFP is mobile in LβT2 cells and it appears to move laterally along the rim. The mobility of AKAP150-GFP was demonstrated in the time-lapse (Figure 4) and FRAP (Figure 11) assays. The decrease in fluorescence intensity in most observed of the cells treated with pharmacological agents in the time lapse assays suggests that AKAP150-GFP was mobile. As a more sensitive system in which to examine the translocation of AKAP150-GFP, we analyzed the mobility of AKAP150-GFP using FRAP. Heat maps created from the FRAP data provided evidence that AKAP150-GFP moved laterally along the cell rim. Not only did the heat maps show recovery within the ROI, the maps demonstrate FLIP outside of the ROI. The fluorescence loss in photobleaching outside of the ROI shows that AKAP150-GFP translocates laterally from outside of the ROI to inside of the ROI during recovery (Figure 9). Results supporting lateral mobility were also observed in the recovery curves. In almost all of the recovery curves, the middle of the ROI recovered slower than the edges of the ROI.

The recovery of AKAP150-GFP could be affected by the higher expression of endogenous AKAP150 and actin within the spots observed in cells immunostained for AKAP150 and actin (Figure 23). The biological nature of the spots is not yet

known. It is possible that the spots provide a barrier or sink to lateral and cytosolic movement during recovery. It is possible that AKAP150 must first bind to the spots before continuing translocation during recovery. When comparing the profile fluorescence intensities of AKAP150 to actin, it appears to be similar. This suggests that AKAP150 could be bound (directly or indirectly) to actin in LβT2 cells. The significant decrease in AKAP150 fluorescence intensity in cells treated with rp-8-cpt-cAMPs or 6-benzoyl-cAMP suggests a change in localization of the scaffolding protein upon the activation or inhibition of PKA (Figure 24). The significant decrease in actin fluorescence intensity in cells treated with 6-benzoyl-cAMP could be occurring due to actin remodeling. In pancreatic β cells, filamentous actin is remodeled before secretion of insulin (Kalwat and Thurmond 2013).

When contemplating how mobility of AKAP150 impacts signaling in LβT2 cells, it is feasible that it adds another level of negative feedback. By removing PKA from its target protein, AKAP150 inhibits the possibility of erroneous, activating phosphorylation. A different way that the mobility of AKAP150 impacts signaling is through signaling cascades. It is imaginable that the scaffolding protein is involved with multiple different signaling cascades. Translocating to different areas in the cell would allow AKAP150 to participate in several pathways. In specific areas of the cell, AKAP150 could bind different enzymes. This would allow AKAP150 to create different changes in the cell based on localization.

While the scanning laser confocal microscope provided conclusive results using the preliminary parameters, we realized increasing temporal resolution is more challenging than anticipated. In order to minimize photobleaching in the cytosol, the

fast rectangular parameters were used during FRAP (Figure13- Figure 16). We predicted this would allow us to identify a difference between cytosolic and lateral recovery. After several FRAP experiments, we realized that the ROI was not uniformly photobleached (Figure 12). Increasing the amount of time photobleached from one second to 2.5 seconds did improve in decreasing fluorescence intensity, but not consistency. Deciding to forgo cytosolic photobleaching in favor of a more consistent decrease in fluorescence intensity, the fast tornado parameters were used during FRAP (Figure 17- Figure 20). Similar to the fast rectangular parameters results, there was inconsistency in the photobleaching when using a tornado ROI. Increasing photobleaching from one second to 2.5 second did improve in decrease fluorescence intensity, but not consistency. These results were substantiated when viewing the tornado ROI intensity profiles (Figure 21). The scanning laser confocal microscope does not provide consistent photobleaching when using the fast rectangle parameters or the fast tornado parameters. Due to inconsistency during photobleaching, the average shape of the ROI is different from what would be ideal (Figure 22). The ideal shape during photobleaching is rectangular, as shown in the red and black intensity profiles in Figure 21. In analyzing data collected from the fast rectangle parameters and the fast tornado parameters, we came to the conclusion that out of the several FRAP movies collected, only a few were useful. The best way to collect data from the fast rectangle or tornado parameters might be to take several FRAP videos and only use the results have a rectangular shaped intensity profile. It is possible that the scanning laser confocal microscope can only produce an adequate decrease in fluorescence intensity when photobleaching for 2.5 seconds.

Future Directions

Since the trend of decreased intensity was observed in almost all of the pharmacological agents used in the time-lapse imaging assays, we want to examine these results further. In order to accomplish this, we will use all of the pharmacological agents in the time-lapse assay during FRAP. Before this can be done, we must determine the best way to collect FRAP data. One possibility is changing the shape of the ROI while using the fast tornado parameters. By increasing the size of the ROI, it is possible to consistently create a rectangular-shaped photobleach, similar to the black intensity profile in Figure 21. Although this would be at the expense of photobleaching more cytosol, we decided it more beneficial to have a consistent ROI. If we could photobleach with the same shaped ROI, we could continue to push temporal resolution. This would allow us to examine recovery after only one second of photobleaching.

Another future direction is focusing on, identifying and finding the significance of the spots in the endogenous AKAP150 staining. By treating the cells with all of the pharmacological agents used in the time-lapse imaging assay, we can compare changes in AKAP150 and actin intensities. This would allow us to determine if the AKAP150 and actin intensities continue to appear to change together. These results could help in determining if AKAP150 attaches (directly or indirectly) to actin. Taking videos of transfected cells without photobleaching will show what is happening to the spots over time. We could determine if the spots change intensity without photobleaching and calculate their recovery rate. Then we could determine if rate of change in the spots is different during photobleaching.

Lastly, we are interested in the changes in cytosolic calcium after treatment with the pharmacological agents in the time-lapse imaging assay. This can be investigated using FURA2-AM in cells transfected with AKAP150-GFP. An increase in cytosolic calcium can indicate the opening of ion channels, leading to the secretion of hormone. If we could determine which pharmacological agents potentially cause opening of ion channels, we could learn more about what causes the translocation of AKAP150-GFP.

BIBLIOGRAPHY

Alberts, B. Johnson, A. Lewis, J. Raff, M. Roberts, K. Walter, P. *Molecular Biology of the Cell, 5th Edition*. N.p., 2008. Print.

Brogi, Simone et al. "Discovery of GPCR Ligands for Probing Signal Transduction Pathways." *Frontiers in pharmacology* 5.November (2014): 255. Web.

Dai, Shuiping, Duane D Hall, and Johannes W Hell. "Supramolecular Assemblies and Localized Regulation of Voltage-Gated Ion Channels." *Physiological reviews* 89.2 (2009): 411–452. Web.

Davis, Shannon W. et al. *Pituitary Gland Development and Disease: From Stem Cell to Hormone Production*. Vol. 106. N.p., 2013. Web

Dell'Acqua, M. L., and J. D. Scott. "Protein Kinase A Anchoring." *Journal of Biological Chemistry* 1997: 12881–12884. Print.

Gao, Tianyan et al. "cAMP-Dependent Regulation of Cardiac L-Type Ca2+ Channels Requires Membrane Targeting of PKA and Phosphorylation of Channel Subunits." *Neuron* 19.1 (1997): 185–196. Web.

Hall, Randy a., and Robert J. Lefkowitz. "Regulation of G Protein-Coupled Receptor Signaling by Scaffold Proteins." *Circulation Research* 91.8 (2002): 672–680. Web.

Hoshi, Naoto, Lorene K Langeberg, and John D Scott. "Distinct Enzyme Combinations in AKAP Signalling Complexes Permit Functional Diversity." *Nature cell biology* 7.11 (2005): 1066–1073. Web.

Kalwat, Michael A, and Debbie C Thurmond. "Signaling Mechanisms of Glucose-Induced F-Actin Remodeling in Pancreatic Islet β Cells." *Experimental & molecular medicine* 45 (2013): e37. Web.

Kobilka, Brian K. "G Protein Coupled Receptor Structure and Activation." *Biochimica biophysica acta* 1768.4 (2007): 794–807. Web.

Liu, Fujun, Darrell A Austin, et al. "GnRH Activates ERK1/2 Leading to the Induction of c-Fos and LHbeta Protein Expression in LbetaT2 Cells." *Molecular*

endocrinology (Baltimore, Md.) 16.3 (2002): 419–434. Print.

Liu, Fujun, Isao Usui, et al. "Involvement of Both Gq/11 and Gs Proteins in Gonadotropin-Releasing Hormone Receptor-Mediated Signaling in L??T2 Cells." *Journal of Biological Chemistry* 277.35 (2002): 32099–32108. Web.

Ooi, Guck T., Neveen Tawadros, and Ruth M. Escalona. "Pituitary Cell Lines and Their Endocrine Applications." *Molecular and Cellular Endocrinology* 228.1-2 (2004): 1–21. Web.

Taskén, Kjetil, and Einar Martin Aandahl. "Localized Effects of cAMP Mediated by Distinct Routes of Protein Kinase A." *Physiological reviews* 84.1 (2004): 137–167. Web.

Thomas, P et al. "The L Beta T2 Clonal Gonadotrope: A Model for Single Cell Studies of Endocrine Cell Secretion." *Endocrinology* 137.7 (1996): 2979–2989. Print.

Tunquist, Brian J et al. "Loss of AKAP150 Perturbs Distinct Neuronal Processes in Mice." *Proceedings of the National Academy of Sciences of the United States of America* 105.34 (2008): 12557–12562. Web

Yeung, Chung M. et al. "Cells of the Anterior Pituitary." *International Journal of Biochemistry and Cell Biology* 38.9 (2006): 1441–1449. Web.